Computers and Chemical Engineering 130 (2019) 106576

Contents lists available at ScienceDirect

Computers and Chemical Engineering

journal homepage: www.elsevier.com/locate/compchemeng

# Dissipativity learning control (DLC): A framework of input–output data-driven control

Wentao Tang, Prodromos Daoutidis*

*Department of Chemical Engineering and Materials Science, University of Minnesota, Minneapolis, MN 55455, U.S.A*

ARTICLE INFO

*Article history:*
Received 4 July 2019
Revised 9 September 2019
Accepted 17 September 2019
Available online 17 September 2019

*Keywords:*
Data-driven control
Dissipative systems
Machine learning

ABSTRACT

The paper addresses data-driven control based on input–output data in the absence of an underlying dynamic model. It proposes a dissipativity learning control (DLC) framework which involves the data-based learning of the dissipativity property of the control system, followed by a dissipativity-based controller design procedure. Specifically, independent component analysis and parametric distribution inference are adopted to estimate a polyhedral region of input–output trajectory samples, whose dual cone characterizes the dissipativity property; subsequently, an optimal controller in the $L_2$ sense is designed by solving a nonlinear semidefinite programming problem. The applicability of the proposed method is demonstrated by case studies on regulating control of a polymerization reactor and tracking control of an oscillatory chemical reactor.



## 1. Introduction

Big data analytics is playing an increasing role in the operations and optimization of chemical process systems (Qin and Chiang, 2019; Venkatasubramanian, 2019). Data-driven control, which aims to design controllers based on historical and/or online operational data provides an alternative to model-based control with the potential of circumventing the difficulties of deriving, identifying, updating, and modifying control-oriented dynamic models (Hou and Wang, 2013). Data-driven modeling approaches, ranging from traditional transfer function identification (Lao et al., 2013), temporal linearization (Chi et al., 2015), regression (Tanaskovic et al., 2017; Narasingam and Kwon, 2018), adaptive parameter estimation (Heirung et al., 2017) and Koopman operators or dynamic mode decomposition (Williams et al., 2015; Proctor et al., 2018; Korda and Mezić, 2018; Narasingam and Kwon, 2019) to artificial neural networks (Aggelogiannaki and Sarimveis, 2008; Mu et al., 2017) and machine learning algorithms (Mesbah, 2018), can in principle be incorporated into model-based control methods to resolve the complexity involved in first-principles modeling. Although intrinsically dependent on data, these approaches are not truly model-free and their efficacy is strongly affected by the complexity and accuracy of the learned surrogate models.

*Model-free data-driven control* approaches have also been developed, mostly based on approximate dynamic programming (ADP). In these approaches, one focuses on the optimal control policy and/or the optimal control cost (or *Q*-function) as state-dependent functions determined by the Hamilton-Jacobi-Bellman (HJB) optimality principle, and obtains their approximations (Lee and Lee, 2005; Lee and Wong, 2010) through either offline regression (Luo et al., 2014; Tang and Daoutidis, 2018) or online iterative schemes under the name of reinforcement learning (RL) (Lillicrap et al., 2015; Spielberg et al., 2019). Instead of obtaining a full dynamic model, in these model-free approaches, one seeks only *essential control-relevant information* (e.g., *Q*-function), thus largely reducing the complexity of designing well-performing controllers. With the development of machine learning, especially deep learning methods (Shin et al., 2019), ADP and RL approaches are expected to find wider applications. However, the application of ADP in process control is still limited to small-scale systems with relatively simple dynamics. This is due to the dependence of ADP formulations on the state-space information of the system, which can be limited for chemical processes. For example, for systems with unobservable states, one does not have access to full state information, and the construction of a model-free state estimator is nontrivial (see, e.g., Ghavamzadeh et al., 2015). Further, in the presence of high-dimensional nonlinear dynamics of the states, it is difficult to choose the approximators of the state-dependent optimal control policy and cost functions. It is clear that so far, a data-driven model-free control framework that applies to process systems with possibly unobservable, high-dimensional, and nonlinearly-related states, remains an open problem.

* Corresponding author.
*E-mail address:* daout001@umn.edu (P. Daoutidis).

https://doi.org/10.1016/j.compchemeng.2019.106576
0098-1354/

**Nomenclature**

*Latin Letters*

| | |
|---|---|
| $a, b, c, w$ | Biexponential distribution parameters |
| $D^+, D^-$ | Scales of biexponential distributions |
| $d$ | Exogenous disturbances |
| $E$ | Basis matrix for symmetric matrices |
| $f, g, h, l$ | Unknown vector fields in the model |
| $I$ | Unit matrix |
| $J$ | Dimension of independent components |
| $K$ | Controller gain matrix |
| $M$ | Mixing matrix |
| $\mathbb{N}$ | Set of positive integers |
| $\mathcal{N}$ | Normal distribution |
| $N$ | Positive integer |
| $P$ | Number of samples |
| $p$ | Constants |
| $q$ | Probability density function |
| $\mathbb{R}$ | Set of real numbers |
| $r$ | Dimension of the dissipativity parameters |
| $\mathbb{S}$ | Set of symmetric matrices |
| $\mathbb{S}_+$ | Set of positive semidefinite matrices |
| $\mathcal{S}$ | Dual dissipativity set |
| $s$ | Supply rate function |
| $T$ | Time duration |
| $t$ | Time variable |
| $U$ | Orstein-Uhlenbeck process |
| $u$ | Control inputs |
| $V$ | Storage function |
| $v$ | Auxiliary variable |
| $W$ | Wiener process |
| $x$ | State variables |
| $y$ | Output variables |
| $z$ | Performance outputs |

*Greek Letters*

| | |
|---|---|
| $\alpha$ | Constants |
| $\beta$ | Upper bound of squared $L_2$-gain |
| $\Gamma$ | Dual dissipativity parameters |
| $\gamma$ | Vectorized dual dissipativity parameters |
| $\Delta$ | Confidence level |
| $\delta$ | Kronecker delta |
| $\epsilon$ | Small real number |
| $\zeta$ | Lumped random variable |
| $\eta$ | Random vectors with independent compoents |
| $\theta$ | Parameter in biexponential distribution |
| $\kappa$ | Control law |
| $\lambda$ | Lagrangian dual |
| $\xi$ | Whitened random vectors |
| $\Pi$ | Dissipativity parameters |
| $\pi$ | Vectorized dissipativity parameters |
| $\rho$ | Eigenvalue |
| $\Sigma$ | Covariance matrix |
| $\sigma$ | Scales of deviations from the contacting endpoint of biexponential distributions |
| $\tau$ | Dummy time variable |
| $\upsilon$ | Magnitude of Orstein-Uhlenbeck process |
| $\omega$ | Inverse time constant of Orstein-Uhlenbeck process |

*Subscripts*

| | |
|---|---|
| $+, -$ | Positive and negative deviations from mean, or positive and negative parts of a real number |
| $i$ | Index of vertices in convex hull |
| $j$ | Index of independent components |
| $k$ | Index of bases |
| P,I,D | Proportional, integral, and differential mode |

*Superscripts*

| | |
|---|---|
| $p$ | Index of samples |

*Other Notations*

| | |
|---|---|
| $^*$ | Dual cone of a set |
| $^\top$ | Transpose of a matrix |
| $\bar{\cdot}$ | Setpoint for tracking |
| $\tilde{\cdot}$ | Deviation from the tracking target |
| $\hat{\cdot}$ | Controller properties |
| $\check{\cdot}$ | Closed-loop properties |
| $[\cdot]$ | The implicit matrix $A$ or vector $a$ in a quadratic form $A^\top BA$ or $a^\top Ba$ |
| $\|\cdot\|$ | Norm |
| $\langle \cdot, \cdot \rangle$ | Inner product of matrices |
| coni | Conic hull |
| conv | Convex hull |
| trace | Matrix trace |

A promising approach to such a framework is to adopt an *input–output* perspective of process systems towards a data-driven control strategy depending only on input and output data without involving any state-space description. To this end, we note that the concept of *dissipativity* (Willems, 1972; Hill and Moylan, 1976; Moylan and Hill, 1978; Hill and Moylan, 1980), as a characterization of input–output behavior, has been widely exploited for output-feedback control (Polushin et al., 2000; Lozano et al., 2013). In the context of model-based control, through a thermodynamic analysis on the dynamic model under certain (rather restrictive) assumptions, the dissipative properties of process systems involving a storage function and a supply rate function can be determined by choosing inputs and outputs consistent with irreversible thermodynamics (Alonso and Ydstie, 1996; Ydstie, 2002; Ruszkowski et al., 2005; Hioe et al., 2013) or adopting a Hamiltonian modeling approach (Hangos et al., 2001; Ramirez et al., 2013; García-Sandoval et al., 2016).

Dissipativity-based control can be naturally extended into an input–output data-driven control strategy, which we call *dissipativity learning control* (DLC). Key to this data-driven framework is the use of machine learning techniques to obtain the dissipative property from data rather than a first-principles model. The learned dissipativity is then combined with a dissipativity-based controller synthesis formulation to obtain a desirable control law. Recently, data-based dissipativity learning approaches have been introduced (Wahlberg et al., 2010; Maupong et al., 2017; Romer et al., 2017); however, these works are restricted to specific simple forms of dissipativity properties or linear dynamics, and are not followed by controller design. In Tang and Daoutidis (2019), we first proposed a dissipativity learning control framework, where a one-class support vector machine for learning the dissipativity property is combined with the controller synthesis. This results in an integrated quadratic and semidefinite programming problem that can be solved via an iterative algorithm, throughout which the dissipativity property is updated until the optimal estimation is approached. However, this procedure is computationally expensive due to the repeated learning, and its performance is dependent on the convergence of the iterative algorithm.

In this work, we propose a more effective approach, where the dissipativity learning and the controller design are carried out successively, thus avoiding the complexity of the iterative algorithm. The learning procedure estimates a *range* of the supply rate, and involves the following three steps: (1) the data samples under the system dynamics are treated with independent component analysis

for dimensionality reduction, (2) bi-exponential distribution inference is performed to obtain a polyhedral confidence region of trajectory data, and (3) a dual polyhedral cone is constructed as the approximate range of the parametric representation of the supply rate function. Based on the estimated range of the supply rate, a controller is designed to minimize an upper bound of the $L_2$-gain by solving a semidefinite programming problem. Such a novel approach can be applied to both regulating and tracking tasks, for the latter of which deviation variables from the time varying input and output trajectories are used instead of deviations from static setpoints.

The remainder of this paper is organized as follows. We first introduce preliminaries of dissipativity and dissipativity-based control in Section 2. The dissipativity learning control framework is proposed in Section 3. We examine the proposed method with case studies on regulating control and tracking control of two different chemical reactors in Section 4 and 5, respectively. Conclusions are given in Sections 6.

## 2. Preliminaries

### 2.1. Dissipativity

Dissipativity is an important characterization of the input–output property of dynamic systems that describes how the states of the system move across the contours of a nonnegative function under the effect of the input and output variables. Dissipativity, as defined by Willems (1972), states that the change of a state-dependent storage function $V(x)$ can not exceed the accumulation of an input and output-dependent supply rate $s(u; y)$.

**Definition 1.** A dynamic system in the general nonlinear form

$$\dot{x} = f(x, u), \quad y = h(x, u). \tag{1}$$

is said to be *dissipative* in the (nonnegative) *storage* function $V(x)$ with respect to the *supply rate* $s(u; y)$ if under the system dynamics (1), the dissipative inequality holds for any input trajectory $u(t)$ on any time interval $[t_1, t_2]$:

$$V(x(t_2)) - V(x(t_1)) \le \int_{t_1}^{t_2} s(u(t); y(t))dt. \tag{2}$$

Generally, the inputs of the plant include not only control inputs $u$ but also disturbances $d$, whose components are assumed to be equal to 0 in the nominal plant. Here we consider plants governed by the following (unknown) input-affine dynamics, where $x$, $u$ and $d$ are vectors:

$$\dot{x} = f(x) + g(x)u + l(x)d. \tag{3}$$

For reference tracking problems, the setpoint trajectories of inputs, $\bar{u}$, and outputs, $\bar{y}$, which satisfy the undisturbed dynamics

$$\dot{\bar{x}} = f(\bar{x}) + g(\bar{x})\bar{u}, \quad \bar{y} = h(\bar{x}), \tag{4}$$

may vary with time. For regulating control, the setpoints are fixed at $\bar{u} = 0$, $\bar{y} = 0$. The setpoint signals are given a priori by a dynamic or static simulator of the plant. Define the deviations of the control inputs and the outputs from the corresponding setpoints as $\tilde{u} := u - \bar{u}$ and $\tilde{y} := y - \bar{y}$, respectively. Thus, the plant is viewed as a mapping $(\tilde{u}, d, \bar{u}) \to \tilde{y}$ with states $\tilde{x}$ and $\bar{x}$:

$$\begin{aligned}
\dot{\tilde{x}} &= f(\bar{x}+\tilde{x}) + g(\bar{x}+\tilde{x})(\bar{u}+\tilde{u}) + l(\bar{x}+\tilde{x})d - f(\bar{x},\bar{u}) - g(\bar{x})\bar{u},\\
\dot{\bar{x}} &= f(\bar{x}) + g(\bar{x})\bar{u},\\
\tilde{y} &= h(\bar{x}+\tilde{x}) - h(\bar{x}).
\end{aligned} \tag{5}$$

We consider the controller as a mapping from the output deviations (errors) and the input setpoints to the input deviations

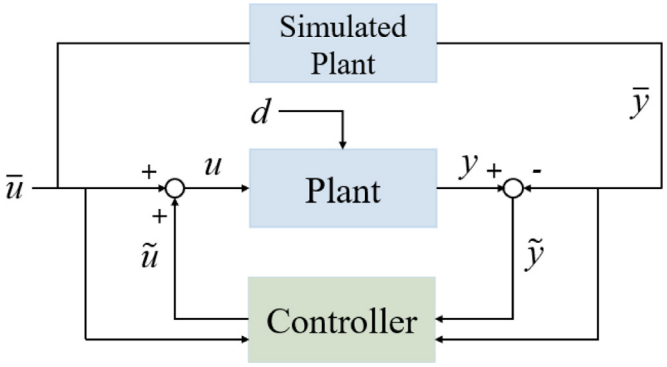


**Fig. 1.** System architecture.

$\kappa : (\tilde{y}, \bar{u}) \to \tilde{u}$ to be designed ($\bar{y}$ is not included since it is determined by $\bar{u}$), i.e., we seek

$$\tilde{u} = \kappa(\tilde{y}, \bar{u}). \tag{6}$$

Hence the closed-loop system is a map from $(d, \bar{u})$ to the tracking errors in both the inputs and the outputs $(\tilde{y}, \tilde{u})$. The architecture of such a control system is illustrated in Fig. 1. Under such an architecture, suppose that the dissipative inequality of the open-loop system (5) is written as

$$V(\tilde{x}(t_2), \bar{x}(t_2)) - V(\tilde{x}(t_1), \bar{x}(t_1)) \le \int_{t_1}^{t_2} s(\tilde{u}(t), d(t), \bar{u}(t); \tilde{y}(t))dt. \tag{7}$$

Substituting the feedback control law (6) into the above formula, we see that the closed-loop system, with $(\tilde{x}, \bar{x})$ as its states, is dissipative with respect to a new supply rate $\check{s}$:

$$s(\kappa(\tilde{y}, \bar{u}), d, \bar{u}; \tilde{y}) =: \check{s}(d, \bar{u}; \tilde{y}). \tag{8}$$

The closed-loop dissipative inequality is naturally connected to Lyapunov stability. Consider the undisturbed case when $d = 0$. If $\check{s}(0, \bar{u}; \tilde{y}) \le 0$, then according to the Krasovskii-LaSalle's principle of invariance (Khalil, 2002), the system states will converge to an invariant set in which the supply rate remains 0 and the storage reaches its minimum. If $\check{s}(0, \bar{u}; \tilde{y}) \le 0$ and the equality holds only when $\tilde{y} = 0$, then the afore-mentioned invariant set is such that the tracking errors become zero, i.e., the output tracking control is realized. If we further assume that (5) is partially observable in $\tilde{x}$, then we realize state tracking. For regulating control, it suffices to have the inequality hold only for $\bar{u} = 0$. When there exist disturbances, the control performance is characterized by the effect of the disturbances on $(\tilde{y}, \tilde{u})$ in the sense of an $L_2$-gain. To this end, we have the following assertion.

**Theorem 1.** *If the closed-loop supply rate $\check{s}(d, \bar{u}; \tilde{y})$ satisfies the bounded nonconcavity condition:*

$$\check{s}(d, \bar{u}; \tilde{y}) \le \beta\|d\|^2 - \|\kappa(\tilde{y}, \bar{u})\|^2 - \|\tilde{y}\|^2, \tag{9}$$

*for a positive real number $\beta$, then the closed-loop system is $L_2$-stable, with an $L_2$-gain (from the disturbances to the input and output tracking errors) no larger than $\beta^{1/2}$.*

**Proof.** With (8) as a supply rate function and the definition of the controller (6), on any time interval $[0, T]$ we have

$$V|_{t=T} - V|_{t=0} \le \int_0^T \check{s}dt \le \int_0^T (\beta\|d\|^2 - \|\tilde{u}\|^2 - \|\tilde{y}\|^2)dt. \tag{10}$$

Rearrange the above formula and relax the non-positive $-V|_{t=T}$ term on the right-hand side to obtain

$$\|\tilde{u}\|^2_{L_2[0,T]} + \|\tilde{y}\|^2_{L_2[0,T]} \le \beta\|d\|^2_{L_2[0,T]} + V|_{t=0}. \tag{11}$$

This conforms to the definition of $L_2$-stability (Khalil, 2002) with an upper bound on the $L_2$-gain of $\beta^{1/2}$. □

This connection between the dissipativity of the closed-loop system and $L_2$-stability is the theoretical basis of dissipativity-based control to be discussed in the next subsection.

### 2.2. Dissipativity-based control

The determination of a supply rate function of the plant satisfying the condition (9), namely the dissipativity learning procedure, will be addressed in the next section. Now we assume that such a function $s$ is known, and consider the problem of synthesizing a feedback controller in the form of (6) with desired closed-loop performance. For simplicity, we assume that the supply rate $s$ is quadratic in $\tilde{u}, d, \tilde{y}$, the feedback law $\kappa$ is linear in $\tilde{y}$, and hence $\check{s}$ is also quadratic in $d, \tilde{u}, \tilde{y}$, namely

$$\begin{aligned} s(\tilde{u}, d, \bar{u}; \tilde{y}) &= [d^\top \quad \tilde{u}^\top \quad \tilde{y}^\top]\Pi(\bar{u})[\cdot], \\ \kappa(\tilde{y}, \bar{u}) &= K(\bar{u})\tilde{y}, \\ \check{s}(d, \bar{u}, \tilde{y}) &= [d^\top \quad (K(\bar{u})\tilde{y})^\top \quad \tilde{y}^\top]\Pi(\bar{u})[\cdot], \end{aligned} \tag{12}$$

where $\Pi(\bar{u})$ is a symmetric matrix called the dissipativity matrix and $K(\bar{u})$ is the feedback gain matrix that may depend on $\bar{u}$. The upper bound of the squared closed-loop $L_2$-gain is estimated by (9), i.e., the smallest positive $\beta$ such that

$$[d^\top \quad (K(\bar{u})\tilde{y})^\top \quad \tilde{y}^\top]\Pi(\bar{u})[\cdot] \le \beta\|d\|^2 - \|K(\bar{u})\tilde{y}\|^2 - \|\tilde{y}\|^2 \tag{13}$$

holds for any $d$, $\tilde{y}$ and $\bar{u}$, i.e., such that

$$\begin{bmatrix} I & 0 & 0 \\ 0 & K(\bar{u})^\top & I \end{bmatrix} \left( \Pi(\bar{u}) + \begin{bmatrix} -\beta I & 0 & 0 \\ 0 & I & 0 \\ 0 & 0 & I \end{bmatrix} \right) \begin{bmatrix} I & 0 \\ 0 & K(\bar{u}) \\ 0 & I \end{bmatrix} \preceq 0. \tag{14}$$

For simplicity, we need to further assume that $\Pi$ and hence $K$ are independent of $\bar{u}$, so that the above semidefinite inequality does not need to be repeated for all possible (or multiple) values of $\bar{u}$. This is equivalent to choosing an overestimate for the supply rate function $s$ within the possible range of $\bar{u}$. This conservatism aims at designing a control law that is dependent only on deviations and invariant to the reference trajectory, and is usually acceptable as long as such a control law gives satisfactory performance. Thus, we consider the $L_2$-optimal dissipativity-based controller design as the problem of finding the controller gain $K$ such that the upper bound of the squared $L_2$-gain $\beta$ is minimized:

$$\begin{aligned} &\min_{K} \quad \beta \\ &\text{s.t.} \quad \begin{bmatrix} I & 0 & 0 \\ 0 & K^\top & I \end{bmatrix} \left( \Pi + \begin{bmatrix} -\beta I & 0 & 0 \\ 0 & I & 0 \\ 0 & 0 & I \end{bmatrix} \right) \begin{bmatrix} I & 0 \\ 0 & K \\ 0 & I \end{bmatrix} \preceq 0. \end{aligned} \tag{15}$$

We note that proportional (P), proportional-integral (PI) and proportional-integral-differential (PID) control laws are the three most classical forms in process control. For implementing PID controllers, we need to augment the plant outputs with their integrals and derivatives, i.e., $(y_\mathrm{P}, y_\mathrm{I}, y_\mathrm{D}) = (y, \int_0^t y(\tau)d\tau, dy/dt)$, and the reference outputs into $(\bar{y}_\mathrm{P}, \bar{y}_\mathrm{I}, \bar{y}_\mathrm{D}) = (\bar{y}, \int_0^t \bar{y}(\tau)d\tau, d\bar{y}/dt)$, so that the feedback signals to the controller include the integral and derivative of $\tilde{y}$ (assuming that the function $h$ is differentiable, so that the time derivatives of $y$ and $\bar{y}$ exist). The augmented outputs can be regarded as the output variables of the corresponding augmented plant dynamics (with auxiliary state variables $v$):

$$\begin{bmatrix} \dot{x} \\ \dot{v} \end{bmatrix} = \begin{bmatrix} f(x,u) \\ h(x) \end{bmatrix}, \quad \begin{bmatrix} y_\mathrm{P} \\ y_\mathrm{I} \\ y_\mathrm{D} \end{bmatrix} = \begin{bmatrix} h(x) \\ v \\ \dfrac{dh(x)}{dx} f(x,u) \end{bmatrix}. \tag{16}$$

Given the dissipativity property of the above augmented dynamics, if we find the optimal controller gain matrix $K$ with augmented outputs, then the matrix can be partitioned into $K = [K_\mathrm{P}, K_\mathrm{I}, K_\mathrm{D}]$ so that the feedback control law is expressed as

$$\tilde{u}(t) = K_\mathrm{P}\tilde{y}(t) + K_\mathrm{I}\int_0^t \tilde{y}(\tau)d\tau + K_\mathrm{D}\frac{d\tilde{y}(t)}{dt}. \tag{17}$$

In this case, the $L_2$-optimal PID controller design results from the following problem modified from (15):

$$\begin{aligned} &\min_{K_\mathrm{P}, K_\mathrm{I}, K_\mathrm{D}} \quad \beta \\ &\text{s.t.} \quad [\cdot]^\top \left( \Pi + \begin{bmatrix} -\beta I & 0 & 0 & 0 & 0 \\ 0 & I & 0 & 0 & 0 \\ 0 & 0 & I & 0 & 0 \\ 0 & 0 & 0 & 0 & 0 \\ 0 & 0 & 0 & 0 & 0 \end{bmatrix} \right) \begin{bmatrix} I & 0 & 0 & 0 \\ 0 & K_\mathrm{P} & K_\mathrm{I} & K_\mathrm{D} \\ 0 & I & 0 & 0 \\ 0 & 0 & I & 0 \\ 0 & 0 & 0 & I \end{bmatrix} \preceq 0, \end{aligned} \tag{18}$$

where $\Pi$ is now a matrix with $5 \times 5$ blocks corresponding to $d$, $\tilde{u}$, $\tilde{y}_\mathrm{P} = \tilde{y}$, $\tilde{y}_\mathrm{I} = \int_0^t \tilde{y}(\tau)d\tau$ and $\tilde{y}_\mathrm{D} = d\tilde{y}/dt$, respectively.

**Remark 1.** Although PID is the most widely used type of controllers in practice, its design or tuning usually requires a transfer function representation of the process. In passivity-based control (Bao and Lee, 2007), a PID controller is proved to be strictly input-passive (i.e., dissipative with respect to a supply rate of $y^\top u - \epsilon\|u\|^2$ for some $\epsilon > 0$) and results in closed-loop stability if the plant is passive (i.e., dissipative with respect to $y^\top u$). However, this has not been discussed in a dissipativity-based control setting, where the plant may have more general forms of supply rate functions. Moreover, an optimal way of designing the PID controller gain matrices is lacking. These issues are addressed by the proposed formulation (18) for the $L_2$-optimal dissipativity-based PID controller design.

## 3. Dissipativity learning control

### 3.1. Dissipativity set and dual dissipativity set

Now we deal with the problem of determining the dissipativity property of the system. We note that to obtain a dissipative inequality, a storage function $V(\bar{x}, \bar{x})$ depending on the states of the system (5) and an input and output dependent supply rate function $s(\tilde{u}(t), d(t), \bar{u}(t); \tilde{y}(t))$ are needed. The involvement of the state-dependent storage function is undesirable since only input and output data are available. This can be avoided by using a theorem similar to the one proved in Hill and Moylan (1976) under the following assumption.

**Assumption 1.** For the system (5), any state $(\bar{x}, \bar{x})$ is reachable in finite time from a state with zero state tracking error, i.e., there exists a finite time $T > 0$ and a trajectory of inputs $(\tilde{u}(t), d(t), \bar{u}(t))$ on $t \in [0, T]$, such that the state at $t = 0$ is $(0, \bar{x}_0)$ for some $\bar{x}_0$, and the state at $t = T$ is $(\bar{x}, \bar{x})$.

This assumption is not restrictive, since the reachability from zero state tracking error is naturally satisfied as long as the system is controllable, which can be usually guaranteed by appropriate control variable selection.

**Theorem 2.** *Suppose that Assumption 1 holds. Then the system (5) is dissipative with respect to $s(\tilde{u}, d, \bar{u}; \tilde{y})$ in a nonnegative storage function $V(\bar{x}, \bar{x})$ satisfying $V(0, \bar{x}) = 0$ for any $\bar{x}$, if and only if for any trajectory starting from any states $(\bar{x}, \bar{x})$ with $\bar{x} = 0$, the following inequality holds*

$$\int_{t_1}^{t_2} s(\tilde{u}(t), d(t), \bar{u}(t); \tilde{y}(t))dt \ge 0. \tag{19}$$

**Proof.** The necessity is evident by using Definition 1. We only prove the sufficiency here. Consider the following function

$$\underline{V}(\tilde{x},\bar{x}) = \inf_{\substack{(\tilde{u}(t),d(t),\bar{u}(t)),\\ \tilde{x}(0)=0,\quad \bar{x}(T)=\bar{x},}} \int_0^T s(\tilde{u}(t),d(t),\bar{u}(t);\tilde{y}(t))dt. \tag{20}$$

According to the reachability assumption 1, the above function is well-defined and finite. If (19) holds, the value of $\underline{V}$ is always non-negative. Consider any trajectory $(\tilde{u}(t),d(t),\bar{u}(t))$ on any time interval $[t_1, t_2]$ and denote the initial and final states as $(\tilde{x}_1,\bar{x}_1)$ and $(\tilde{x}_2,\bar{x}_2)$, respectively. We then have

$$\underline{V}(\tilde{x}_2,\bar{x}_2) - \underline{V}(\tilde{x}_1,\bar{x}_1) = \inf_{\substack{(\tilde{u}(t),d(t),\bar{u}(t)),\\ \tilde{x}(0)=0,\quad \bar{x}(T_2)=\bar{x}_2,}} \int_0^{T_2} sdt - \inf_{\substack{(\tilde{u}(t),d(t),\bar{u}(t)),\\ \tilde{x}(0)=0,\quad \bar{x}(T_1)=\bar{x}_1,}} \int_0^{T_1} sdt, \tag{21}$$

where the first infimum can be relaxed with any trajectory starting from a point with zero tracking error, passing $(\tilde{x}_1,\bar{x}_1)$, and extended by the given trajectory from $(\tilde{x}_1,\bar{x}_1)$ to $(\tilde{x}_2,\bar{x}_2)$. Hence

$$\underline{V}(\tilde{x}_2,\bar{x}_2) - \underline{V}(\tilde{x}_1,\bar{x}_1) \le \int_{t_1}^{t_2} s(\tilde{u}(t),d(t),\bar{u}(t);\tilde{y}(t))dt. \tag{22}$$

According to Definition 1, the system (5) is then dissipative in the storage function $\underline{V}$ with respect to $s$. □

Under the quadratic form of supply rate

$$s(\tilde{u},d,\bar{u};\tilde{y}) = [d^\top \quad \tilde{u}^\top \quad \tilde{y}^\top]\Pi[\cdot], \tag{23}$$

the inequality condition (19) becomes

$$\int_{t_1}^{t_2}[d^\top(t) \quad \tilde{u}^\top(t) \quad \tilde{y}^\top(t)]\Pi[\cdot]dt = \langle \Pi, \int_{t_1}^{t_2}[\cdot][d^\top \quad \tilde{u}^\top \quad \tilde{y}^\top]dt\rangle \ge 0, \tag{24}$$

where the inner product between any two symmetric matrices $\langle\cdot,\cdot\rangle$ is specified as the trace of their product. Practically, we limit (24) to trajectories on which $d$ and $\tilde{u}$ belong to the $L_{2e}$ class (i.e., are finite-time square integrable), so that the integral term in the inner product is finite.

Now we give the key definitions that will be used for dissipativity learning.

**Definition 2.** The *dual dissipativity parameter* of each trajectory $(\tilde{u}(t),d(t),\bar{u}(t),\tilde{y}(t))$, $t\in[t_1, t_2]$ is defined as

$$\Gamma = \int_{t_1}^{t_2}[\cdot][d(t)^\top \quad \tilde{u}(t)^\top \quad \tilde{y}(t)^\top]dt. \tag{25}$$

The collection of dual dissipativity parameters of all the trajectories that start from any $(\tilde{x},\bar{x})$ with $\tilde{x}=0$ and are $L_{2e}$ (quadratically integrable on any finite time interval) in the inputs $(d,\tilde{u})$ is called the *dual dissipativity set*, denoted as $\mathcal{S}$. The dual cone of the dual dissipativity set $\mathcal{S}$,

$$\mathcal{S}^* = \{\Pi \,|\, \langle\Pi,\Gamma\rangle \ge 0, \forall\Gamma\in\mathcal{S}\}, \tag{26}$$

is called the *dissipativity set*. We also define the dissipativity parameter of the system as the matrix $\Pi$ in the supply rate (23).

Then it directly follows from Theorem 2 that the dissipativity set $\mathcal{S}^*$ defined above is the range of the dissipativity parameters. This is stated as the following corollary.

**Corollary 1.** *Suppose that Assumption 1 holds. If $\Pi\in\mathcal{S}^*$, then the system (5) is dissipative with respect to $s(\tilde{u},d,\bar{u};\tilde{y}) = [d^\top \quad \tilde{u}^\top \quad \tilde{y}^\top]\Pi[\cdot]$.*

Hence, the problem of dissipativity learning refers to the determination of the dissipativity set $\mathcal{S}^*$, which requires only to determine the dual dissipativity set $\mathcal{S}$ – the collection of all possible dual dissipativity parameters $\Gamma$.

In a model-free setting, the dual dissipativity set $\mathcal{S}$ is constructed by inference from data. Specifically, we collect $P$ independent samples of trajectories $(\tilde{u}^p(t),d^p(t),\bar{u}^p(t);\tilde{y}^p(t))$, $t\in[t_1^p,t_2^p]$, $p=1,2,\ldots,P$ by randomly generating $L_{2e}$-class inputs $(d,\tilde{u},\bar{u})$ and simulating the system dynamics (5). Then we calculate for each trajectory sample the corresponding dual dissipativity parameter

$$\Gamma^p = \int_{t_1^p}^{t_2^p}[\cdot][d^p(t)^\top \quad \tilde{u}(t)^\top \quad \tilde{y}^p(t)^\top]dt \in \mathcal{S}. \tag{27}$$

Then $\Gamma^p$, $p=1,\ldots,P$ are samples of a random distribution whose support set (the set on which the probability density is nonzero) is $\mathcal{S}$, as long as the input trajectories are sampled from the $L_{2e}$ class, i.e., any $L_{2e}$ signal has a chance of being chosen. This can in principle be realized, for example as in the present paper, using independent Wiener processes of random magnitudes or Orstein-Uhlenbeck processes, although the optimal or near-optimal sampling methods of input trajectories remain an important open problem. Now the dissipativity learning is formally expressed as the following problem:

**Problem 1.** Given samples $\Gamma^p$, $p=1,2,\ldots,P$, infer the support set $\mathcal{S}$ of the underlying distribution of the samples, and explicitly characterize its dual cone $\mathcal{S}^*$.

### 3.2. Dissipativity learning approach

To estimate $\mathcal{S}$, one may directly apply a probability density estimation scheme (see, e.g., Parzen 1962) or kernel (Schölkopf and Smola, 2002) or deep (Ruff et al., 2018) one-class support vector machine algorithms. However, the shape of such an estimated $\mathcal{S}$ can be too complex to explicitly characterize its dual cone $\mathcal{S}^*$ and use it for a subsequent dissipativity-based control mainly due to its non-convexity. In fact, it suffices to obtain a convex hull of $\mathcal{S}$:

$$\mathrm{conv}(\mathcal{S}) = \left\{\sum_{i=1}^N \alpha_i\Gamma_i \,\middle|\, \sum_{i=1}^N \alpha_i = 1, \begin{matrix}\alpha_i\ge 0, \Gamma_i\in\mathcal{S}\\ i=1,2,\ldots,N, N\in\mathbb{N}\end{matrix}\right\} \supseteq \mathcal{S} \tag{28}$$

since the dissipativity set that we aim to find, $\mathcal{S}^*$, is also the dual cone of $\mathrm{conv}(\mathcal{S})$ ($\mathcal{S}^* = \mathrm{conv}(\mathcal{S})^*$). Therefore in this work, we will estimate $\mathcal{S}$ as a *polyhedron*, which can be viewed as the simplest form of convex sets, from trajectory samples.

The key idea underlying the polyhedral estimation is to assume that *the components of $\Gamma$ form a random vector subject to a linear mixture of independent bi-exponential distributions, so that its confidence regions yield polyhedral approximations of its support set*, and that such a mixture of bi-exponential distributions can be inferred through *independent component analysis* (ICA) and *parametric statistical inference* of the component distributions. Here we first represent the matrix $\Gamma$ and $\Pi$ isomorphically as vectors $\gamma$ and $\pi$, respectively, by choosing an orthonormal basis in the corresponding matrix space $\{E_k\}$, so that $\langle\Pi,\Gamma\rangle = \pi^\top\gamma$, i.e.,

$$\Gamma = \sum_k \gamma_k E_k, \quad \Pi = \sum_k \pi_k E_k; \qquad \gamma_k = \langle\Gamma,E_k\rangle, \quad \pi_k = \langle\Pi,E_k\rangle. \tag{29}$$

By vectorizing all the samples to $\gamma^p$, $p=1,\ldots,P$, Problem 1 is restated as

**Problem 2.** Given samples $\gamma^p$, $p=1,\ldots,P$, find the underlying independent components and infer their bi-exponential distributions, thus explicitly characterizing any confidence set as a polyhedron and its dual cone.

ICA aims to determine a linear transformation of the translated data samples:

$$\gamma^p = \bar{\gamma} + M\eta^p, \quad p = 1, 2, \ldots, P \tag{30}$$

such that $\eta^p$, $p = 1, \ldots, P$ can be viewed as samples of a random vector $\eta$ whose components $\eta_j$, $j = 1, \ldots, J$ are independent with zero means and unit variances. $\bar{\gamma} = \frac{1}{P}\sum_{p=1}^{P}\gamma^p$ is the average of all samples. The classical algorithm (based on kurtosis maximization of $\eta$) was introduced in Hyvärinen and Oja (2000), to which the readers are referred for details. The dimension of the independent components, denoted by $J$, is a tunable hyperparameter.

After the ICA processing, we estimate the bi-exponential distribution of each independent component $\eta_j$, whose samples are $\eta_j^p$, $p = 1, \ldots, P$. Specifically, we suppose that the probability density function of $\eta_j$ as a random variable is a linear combination of two exponential distributions that have a contacting endpoint, opposite directions, and weights summing up to 1:

$$q_j(\eta_j) = \begin{cases} w_j a_j \exp[-a_j(\eta_j - c_j)], & \eta_j \geq c_j \\ (1-w_j) b_j \exp[-b_j(c_j - \eta_j)], & \eta_j < c_j \end{cases} \tag{31}$$

where $a_j > 0$, $b_j > 0$, $c_j$, $0 < w_j < 1$ are 4 parameters constrained by the following 3 equalities:

$$\begin{aligned} \lim_{\eta_j \to c_j^-} q_j(\eta_j) - \lim_{\eta_j \to c_j^+} q_j(\eta_j) &= 0 \quad \text{(continuity)}; \\ \int_{-\infty}^{+\infty} \eta_j q_j(\eta_j) d\eta_j &= 0 \quad \text{(zero mean)}; \\ \int_{-\infty}^{+\infty} \eta_j^2 q_j(\eta_j) d\eta_j &= 1 \quad \text{(unit variance)}. \end{aligned} \tag{32}$$

One can verify that the only one remaining degree of freedom can be represented by a parameter $\theta_j \in [-\pi/4, \pi/4]$, with the following expressions relating $a_j$, $b_j$, $c_j$, $w_j$ to $\theta_j$:

$$\begin{aligned} &a_j = 1/\sin(\pi/4 - \theta_j), \quad b_j = 1/\sin(\pi/4 + \theta_j), \\ &c_j = \sqrt{2}\sin\theta_j, \quad w_j = (1 - \tan\theta_j)/2. \end{aligned} \tag{33}$$

The bi-exponential distribution (31) is hence

$$q_j(\eta_j) = \frac{1}{\sqrt{2}\cos\theta_j} \exp\left[ -\frac{(\eta_j - \sqrt{2}\sin\theta_j)_+}{\sin(\pi/4 - \theta_j)} - \frac{(\eta_j - \sqrt{2}\sin\theta_j)_-}{\sin(\pi/4 + \theta_j)} \right], \tag{34}$$

where the subscripts + and - for any real number stand for its positive and negative parts, respectively, namely $p_+ = \max(0, p)$, $p_- = -\min(0, p)$, $p \in \mathbb{R}$. We use the maximum (logarithmic) likelihood estimation to optimize the value of $\theta$ in the distribution, i.e.,

$$\begin{aligned} \theta_j = \arg\min \quad & [\ln(\sqrt{2}\cos\theta_j) \\ & + \frac{1}{P}\sum_{p=1}^{P} \frac{(\eta_j^p - \sqrt{2}\sin\theta_j)_+}{\sin(\pi/4 - \theta_j)} + \frac{1}{P}\sum_{p=1}^{P} \frac{(\eta_j^p - \sqrt{2}\sin\theta_j)_-}{\sin(\pi/4 + \theta_j)} ]. \end{aligned} \tag{35}$$

With the distributions pf the independent components determined, we clearly see that

$$\zeta = \frac{1}{J}\sum_{j=1}^{J} \left[ \frac{(\eta_j - \sqrt{2}\sin\theta_j)_+}{\sin(\pi/4 - \theta_j)} + \frac{(\eta_j - \sqrt{2}\sin\theta_j)_-}{\sin(\pi/4 + \theta_j)} \right] \tag{36}$$

as an average of $J$ independent variables, each subject to an exponential distribution of parameter 1 (see (34)), is subject to the Erlang distribution whose probability density and cumulative density functions are

$$q(\zeta) = \frac{J^J \zeta^{J-1} \exp(-J\zeta)}{(J-1)!}, \quad Q(\zeta) = 1 - \sum_{k=0}^{J-1} \frac{1}{J!}(J\zeta)^k \exp(-J\zeta) \tag{37}$$

respectively, with a mean of 1 and a variance of $1/J$. When $J$ is large, the central limit theorem dictates that the distribution $Q$ is well approximated by a normal distribution $\mathcal{N}(1, J^{-1/2})$. By letting $Q(\zeta) \leq 1 - \epsilon$ for a small positive number $\epsilon$, we obtain a confidence set

$$\sum_{k=0}^{J-1} \frac{1}{J!}(J\zeta)^k \exp(-J\zeta) \geq \epsilon \xrightarrow{\text{denoted as}} \zeta \leq 1 + J^{-1/2}\Delta, \tag{38}$$

in which $1 - \epsilon$ or $\Delta$ characterizes the confidence level. In reality, due to the discrepancy between the empirical distribution of $\zeta$ obtained from data samples and the assumed Erlang distribution, such a confidence level $\Delta$ needs to be chosen according to a specific portion (e.g., 90% or 95%) of the samples.

By combining the ICA transformation (30) and the construction of the Erlang-distributed random variable (36), we have a polyhedral approximation of the dual dissipativity set:

$$\begin{aligned} \mathcal{S}_\Delta = \Bigg\{ & \gamma \,|\, \gamma = \bar{\gamma} + M\eta, \\ & \frac{1}{J}\sum_{j=1}^{J} \left[ \frac{(\eta_j - \sqrt{2}\sin\theta_j)_+}{\sin(\pi/4 - \theta_j)} + \frac{(\eta_j - \sqrt{2}\sin\theta_j)_-}{\sin(\pi/4 + \theta_j)} \right] \leq 1 + J^{-1/2}\Delta \Bigg\}. \end{aligned} \tag{39}$$

Denote by $c$ the $J$-dimensional vector whose $j$-th component is $\sqrt{2}\sin\theta_j$, $D^+$ and $D^-$ the diagonal matrix of bi-exponential scales whose $j$-th diagonal entry is $\sin(\pi/4 - \theta_j)$ and $\sin(\pi/4 + \theta_j)$, respectively. Denote by $\mathbf{1}$ and $\mathbf{0}$ the vector with all components equal to 1 and 0, respectively. Then by using the variables $\sigma^+$ and $\sigma^-$ representing the scales of deviations from the contacting endpoint $c$ of the bi-exponential distributions, we have

$$\begin{aligned} \mathcal{S}_\Delta = \{ & \gamma \,|\, \gamma = \bar{\gamma} + M(c + D^+\sigma^+ - D^-\sigma^-), \\ & \mathbf{1}^\top\sigma^+ + \mathbf{1}^\top\sigma^- \leq J + J^{1/2}\Delta, \sigma^+ \geq \mathbf{0}, \sigma^- \geq \mathbf{0} \}. \end{aligned} \tag{40}$$

Finally, the dissipativity set $\mathcal{S}^*$ is estimated by the dual cone of $\mathcal{S}_\Delta$, calculated using linear duality theory,

$$\begin{aligned} \mathcal{S}_\Delta^* = \{ & \pi \,|\, \exists\lambda \geq 0, \text{ s.t. } \pi^\top(\bar{\gamma} + Mc) \geq \lambda(J + J^{1/2}\Delta), \\ & (MD^+)^\top\pi \geq -\lambda\mathbf{1}, (MD^-)^\top\pi \leq \lambda\mathbf{1} \}. \end{aligned} \tag{41}$$

Our proposed dissipativity learning method is illustrated in Fig. 2. The algorithmic steps are represented by the blue arrows, namely the ICA, the inference of bi-exponential distributions for independent components, and lumping of the independent components into a one-dimensional random variable $\zeta$. By picking a confidence interval of $\zeta$, a polyhedral estimation of $\mathcal{S}$ is acquired by the inverse reasoning steps represented by the green arrows. The learning procedure depends on only two hyperparameters – the number of independent components $J$ and the confidence level $\Delta$.

**Remark 2.** As will be shown in later case studies, the number of independent components $J$ is determined through a trial-and-error approach to eliminate too large and too small choices that give either overly conservative or loose estimations of the dissipativity property. We note that under different choices of orthonormal basis $\{E_k\}$ to vectorize $\Pi$ and $\Gamma$, the linear transformation linking the groups of basis will be compensated in the mixing matrix $M$ in the ICA step. Hence the dual dissipativity set $\mathcal{S}_\Delta$ and dissipativity set $\mathcal{S}_\Delta^*$, if expressed in terms of the original $\Gamma$ and $\Pi$ matrices rather than vectorized $\gamma$ and $\pi$, will be invariant to the choice of basis. In other words, the choice of orthonormal basis $\{E_k\}$ can be arbitrary.

**Remark 3.** Since $\mathcal{S}^* = \text{coni}(\mathcal{S})^*$, where $\text{coni}(\mathcal{S})$ is the conic hull of $\mathcal{S}$:

$$\begin{aligned} \text{coni}(\mathcal{S}) &= \left\{ \sum_{i=1}^{N} \alpha_i \Gamma_i \,\middle|\, \begin{matrix} \alpha_i \geq 0, \Gamma_i \in \mathcal{S} \\ i = 1, 2, \ldots, N, N \in \mathbb{N} \end{matrix} \right\} \\ &= \{ p\Gamma \,|\, p \geq 0, \Gamma \in \text{conv}(\mathcal{S}) \} \supseteq \text{conv}(\mathcal{S}) \supseteq \mathcal{S}, \end{aligned} \tag{42}$$

one may seek to estimate a conic estimation of the dual dissipativity set instead of a bounded polyhedral one as we have done in

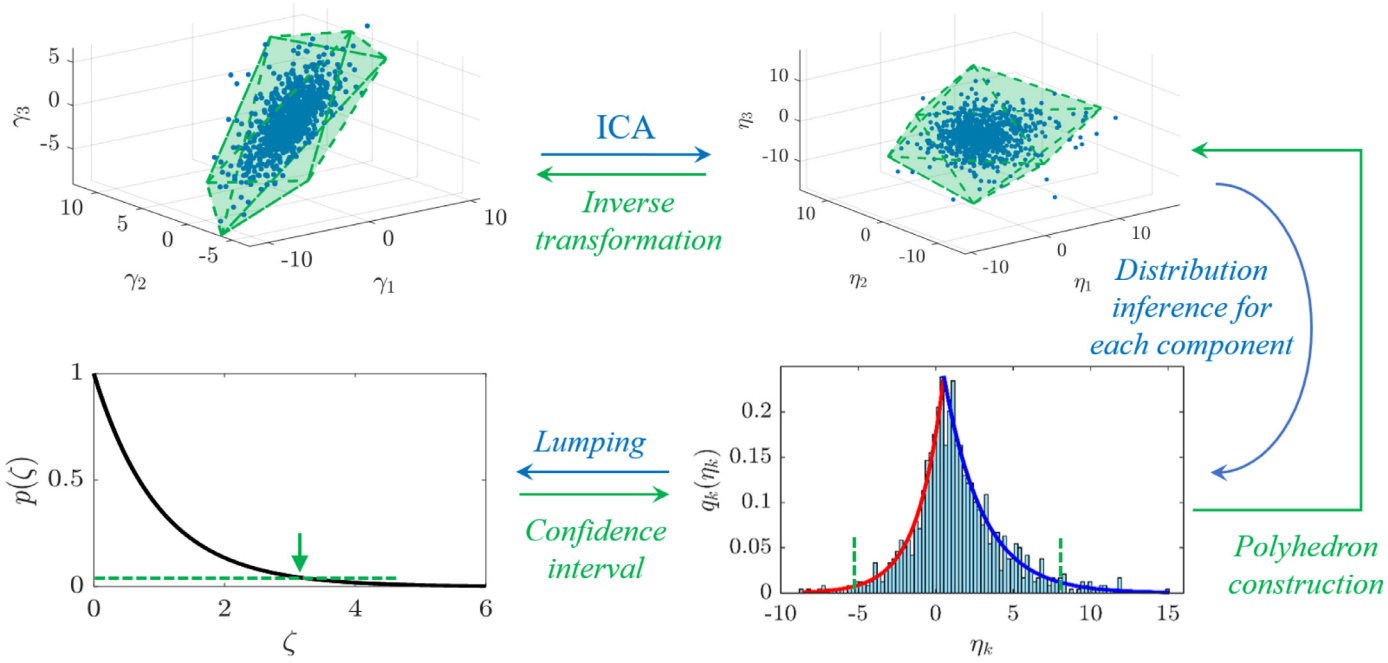


**Fig. 2.** Illustration of the proposed dissipativity learning method.

the main text. This can be done by first scaling the samples onto an affine subspace with a magnitude restriction (e.g., the set of matrices with trace 1), which specifies a section of the conic estimation, and then inferring a polyhedron on this affine subspace. Compared to a polyhedral estimation that is compact in space, the conic counterpart better reflects the intrinsic unboundedness of the dual dissipativity set, as we may have trajectories with sufficiently large input and output signals. However, these trajectories with too large inputs and outputs may not be of interest to characterize system behavior for control purposes, and we tend to avoid them in the data generation procedure due to numerical issues or simulation validity.

**Remark 4.** The ICA and distribution inference approach proposed here for constructing the polyhedral estimation of the dual dissipativity set is motivated by the approach of Zhang et al. (2016) to approximate the feasible region of optimization problems for establishing surrogate models, where convex hulls of data points sampled from the region are found and refined, and the work of Ning and You (2018) to construct the polyhedral uncertainty set for robust optimization, which involves a PCA and a nonparametric distribution inference by kernel smoothing.

**Remark 5.** The assumption of bi-exponential distributions of independent components of $\eta$ can be replaced by bi-normal distributions

$$q_j(\eta_j) = \begin{cases} \frac{w_j}{\sqrt{2\pi}a_j} \exp\left[-\frac{(\eta_j - c_j)^2}{2a_j^2}\right], & \eta_j \geq c_j \\ \frac{1-w_j}{\sqrt{2\pi}b_j} \exp\left[-\frac{(c_j - \eta_j)^2}{2b_j^2}\right], & \eta_j < c_j \end{cases} \tag{43}$$

which gives confidence regions that are linearly transformed ellipsoids following our procedures.

### 3.3. Dissipativity learning control

The dissipativity learning controller design problem can be derived by incorporating the dissipativity set estimation (41) into the $L_2$-optimal control formulation (15). However, the trajectory samples are generated on a *finite* time interval, and, although starting with zero tracking error, they end up *finitely distant* from the target trajectory. As a result, the dissipativity parameters learned based on trajectories away from the target may fail to characterize the system behavior near the target and guide us to a stabilizing controller. Therefore, in addition to the previously constructed estimation of the dissipativity set, we need an additional constraint that requires the dissipativity parameters to satisfy the condition (19) for infinitesimal trajectories starting from zero tracking error. Apparently, it suffices that the submatrix of $\Pi$ corresponding to inputs $(d, \tilde{u})$ be positive semidefinite. This means that when the tracking error is zero, the storage function has reached its minimum and any nonzero control inputs or disturbances will increase the storage function. Thus we have reached the following formulation of dissipativity learning control:

$$\begin{aligned} \min_{\Pi, K, \beta} \quad & \beta \\ \text{s.t.} \quad & \begin{bmatrix} I & 0 & 0 \\ 0 & K^\top & I \end{bmatrix} \left( \Pi + \begin{bmatrix} -\beta I & 0 & 0 \\ 0 & I & 0 \\ 0 & 0 & I \end{bmatrix} \right) \begin{bmatrix} I & 0 \\ 0 & K \\ 0 & I \end{bmatrix} \preceq 0 \\ & \Pi_{d\tilde{u}, d\tilde{u}} \succeq 0, \quad \Pi \in \mathcal{S}^*. \end{aligned} \tag{44}$$

Substituting the true dissipativity set $\mathcal{S}$ with the learned polyhedral conic approximation $\mathcal{S}^*_\Delta$ (41), and expanding the descriptive definition of $\mathcal{S}^*_\Delta$ combined with the basis expansion (29), the formulation becomes

$$\begin{aligned} \min_{\Pi, \pi, K, \lambda, \beta} \quad & \beta \\ \text{s.t.} \quad & \begin{bmatrix} I & 0 & 0 \\ 0 & K^\top & I \end{bmatrix} \left( \Pi + \begin{bmatrix} -\beta I & 0 & 0 \\ 0 & I & 0 \\ 0 & 0 & I \end{bmatrix} \right) \begin{bmatrix} I & 0 \\ 0 & K \\ 0 & I \end{bmatrix} \preceq 0 \\ & \Pi_{d\tilde{u}, d\tilde{u}} \succeq 0, \quad \Pi = \sum_k \pi_k E_k \\ & \lambda \geq 0, \quad \pi^\top (\bar{\gamma} + Mc) \geq \lambda (J + J^{1/2} \Delta) \\ & (MD^+)^\top \pi \geq -\lambda \mathbf{1}, \quad (MD^-)^\top \pi \leq \lambda \mathbf{1}. \end{aligned} \tag{45}$$

**Remark 6.** It is not hard to see that if the Assumption 1 on the reachability of any state from a state of zero tracking error does

not hold, the above-mentioned formulation can still be utilized to obtain an $L_2$-optimal controller that works as long as the initial state of the plant is reachable from a hypothetical state of zero tracking error under some input trajectories.

The above formulation is a non-convex semidefinite programming problem, which can not be simplistically tackled by the available convex optimization solvers such as `cvx` (Grant and Boyd, 2014). The non-convexity arises from the trilinear semidefinite inequality involving the controller gains $K$ twice together with the dissipativity parameters $\Pi$ and upper bound of squared $L_2$-gain $\beta$. However, the problem is multi-convex – once $K$ is fixed, the rest of the problem on ($\Pi$, $\pi$, $\lambda$, $\beta$) is convex; once ($\Pi$, $\pi$, $\lambda$, $\beta$) is fixed, as long as $\Pi_{d\tilde{u},d\tilde{u}} \succeq 0$ is satisfied, we have $\Pi_{\tilde{u},\tilde{u}} \succeq 0$ and hence the remaining problem on $K$ is a convex (quadratic) feasibility problem. We therefore adopt an iterative algorithm to solve (45), where each iteration involves the following two steps:

(a) fix $K$ to solve ($\Pi$, $\pi$, $\lambda$, $\beta$) to the optimum;
(b) seek a different $K$ satisfying the first constraint of (45), so that after changing $K$ the solution obtained in step (a) is still feasible.

When we execute step (a) in the next iteration, the $\beta$ is updated from the previous feasible solution to the optimum under the new $K$. Therefore, the iterations of steps (a) and (b) lead to a sequence of feasible solutions with non-increasing values of $\beta$. Specifically, since the left-hand side of the first constraint of (45) is dependent on $K$ through its bottom right principal minor, $K^\top(\Pi_{\tilde{u},\tilde{u}}+I)K + K^\top\Pi_{\tilde{u},\tilde{y}} + \Pi_{\tilde{u},\tilde{y}}K + (\Pi_{\tilde{y},\tilde{y}}+I)$, which is a quadratic form of $K$, the different $K$ in step (b) can always be chosen as the one such that the quadratic form is the most negative definite. In other words, step (b) updates $K$ according to

$$K = -(\Pi_{\tilde{u},\tilde{u}}+I)^{-1}\Pi_{\tilde{u},\tilde{y}}. \tag{46}$$

If the quantities $M$, $D^+$, $D^-$, $c$ are obtained from the ICA using the $\tilde{u}$ and $(\tilde{y}_\mathrm{P}, \tilde{y}_\mathrm{I}, \tilde{y}_\mathrm{D})$ as inputs and outputs, the formulation (45) can also be extended to an $L_2$-optimal dissipativity learning PID controller:

$$\begin{aligned}
\min_{\Pi,\pi,K,\lambda,\beta}\ & \beta \\
\text{s.t.}\ & [\cdot]^\top\left(\Pi + \begin{bmatrix} -\beta I & 0 & 0 & 0 & 0 \\ 0 & I & 0 & 0 & 0 \\ 0 & 0 & I & 0 & 0 \\ 0 & 0 & 0 & 0 & 0 \\ 0 & 0 & 0 & 0 & 0 \end{bmatrix}\right)\begin{bmatrix} I & 0 & 0 & 0 \\ 0 & K_\mathrm{P} & K_\mathrm{I} & K_\mathrm{D} \\ 0 & I & 0 & 0 \\ 0 & 0 & I & 0 \\ 0 & 0 & 0 & I \end{bmatrix} \preceq 0 \\
& \Pi_{d\tilde{u},d\tilde{u}} \succeq 0, \quad \Pi = \sum_k \pi_k E_k \\
& \lambda \geq 0, \quad \pi^\top(\bar{\gamma} + Mc) \geq \lambda(J + \Delta J^{1/2}) \\
& (MD^+)^\top\pi \geq -\lambda\mathbf{1}, \quad (MD^-)^\top\pi \leq \lambda\mathbf{1}.
\end{aligned} \tag{47}$$

The solution algorithm has no formal difference expect that the update of $K = [K_\mathrm{P}, K_\mathrm{I}, K_\mathrm{D}]$ is expressed as $K = -(\Pi_{\tilde{u},\tilde{u}} + I)^{-1}\Pi_{\tilde{u},\tilde{y}_\mathrm{P}\tilde{y}_\mathrm{I}\tilde{y}_\mathrm{D}}$.

**Remark 7.** Although the properties of multiconvex optimization algorithms have been discussed in some recent works (see, e.g., Shen et al., 2017), it appears that the theoretic convergence of the above algorithm using simple iterations is an open problem. However, likely due to the exploitation of the quadratic constraint on $K$, our algorithm achieves very fast practical convergence (within 20 iterations for the case studies in the following sections), and is therefore suitable for use.

We summarize the entire procedure of dissipativity learning control as follows.

1. Preliminaries.
   (a) Generate data samples.
   (b) Calculate dissipativity parameter samples $\Gamma^p$, $p = 1, 2, \ldots, P$ according to (27).
   (c) Choose orthonormal matrix bases $\{E_k\}$ and vectorize the $\Gamma^p$ into $\gamma^p$ according to (29).
   (d) Set the number of independent components $J$ and confidence level $\Delta$.
   (e) Initialize controller gains $K$.
2. Dissipativity learning.
   (a) Perform ICA and return average $\bar{\gamma}$, mixing matrix $M$ and transformed samples $\eta^p$ in (30).
   (b) For each component $j$, optimize the maximum likelihood estimate of the parameter $\theta_j$ through (35).
   (c) Obtain vector $c$ with components $c_j = [\sqrt{2}\sin\theta_j]$, and matrices $D^+ = \mathrm{diag}(1/\sin(\pi/4 - \theta_j))$, and $D^- = \mathrm{diag}(1/\sin(\pi/4 + \theta_j))$.
3. Controller design.
   (a) With fixed $K$, solve (45) for P control or (47) for PID control and update ($\Pi$, $\pi$, $\lambda$, $\beta$).
   (b) With fixed ($\Pi$, $\pi$, $\lambda$, $\beta$), update $K$ by $K = -(\Pi_{\tilde{u},\tilde{u}} + I)^{-1}\Pi_{\tilde{u},\tilde{y}}$ for P control and $K = -(\Pi_{\tilde{u},\tilde{u}} + I)^{-1}\Pi_{\tilde{u},\tilde{y}_\mathrm{P}\tilde{y}_\mathrm{I}\tilde{y}_\mathrm{D}}$ for PID control.
   (c) If the updated $K$ does not have a sufficiently small deviation from the previous $K$, return to (a) to iterate. Otherwise terminate.

## 4. Case study: Dissipativity learning regulating control of a polymerization reactor

In this section we perform a case study of our proposed dissipativity learning control method on a continuously stirred tank reactor (CSTR) with exothermic polymerization reactions of methyl methacrylate taking place, which was used as a benchmark for nonlinear geometric control (Daoutidis et al., 1990; Soroush and Kravaris, 1992) due to its highly nonlinear dynamics. Here we consider the regulating control of such a reactor ($\tilde{u} = 0$, $\tilde{y} = 0$) since the polymerization extent needs to be held constant for the polymer product.

### 4.1. System description

The system model involves 6 states, 2 inputs, 2 outputs and 2 exogenous disturbances. The 6 states represent the monomer and initiator concentrations, reactor and jacket temperatures, amount of substance and mass of the product. The initiator feed and the cold water flow rates are used as control inputs ($u_1 = F_\mathrm{i}$, $u_2 = F_\mathrm{w}$). The average molecular weight and temperature are outputs ($y_1 = D_1/D_0$, $y_2 = T$, where $D_0$ and $D_1$ are the molar and mass concentration of the polymer products, respectively). There are two disturbances – monomer concentration and temperature of the feed stream ($d_1 = C_{\mathrm{m,in}}$, $d_2 = T_\mathrm{in}$).

The governing equations are given as follows:

$$\begin{aligned}
\dot{C}_\mathrm{m} &= -(k_\mathrm{p} + k_\mathrm{m})C_\mathrm{m}\phi + \frac{F}{V}(C_{\mathrm{m,in}} - C_\mathrm{m}) \\
\dot{C}_\mathrm{i} &= -k_\mathrm{i}C_\mathrm{i} + \frac{F_\mathrm{i}C_{\mathrm{i,in}} - FC_\mathrm{i}}{V} \\
\dot{T} &= k_\mathrm{p}C_\mathrm{m}\phi\frac{-\Delta H_\mathrm{p}}{\rho c_p} - \frac{UA}{\rho c_p V}(T - T_\mathrm{j}) + \frac{F}{V}(T_\mathrm{in} - T) \\
\dot{T}_\mathrm{j} &= \frac{F_\mathrm{w}}{V_\mathrm{w}}(T_\mathrm{w} - T_\mathrm{j}) + \frac{UA}{\rho_\mathrm{w}c_\mathrm{w}V_\mathrm{w}}(T - T_\mathrm{j}) \\
\dot{D}_0 &= \left(\frac{1}{2}k_\mathrm{c} + k_\mathrm{d}\right)\phi^2 + k_\mathrm{m}C_\mathrm{m}\phi - \frac{FD_0}{V} \\
\dot{D}_1 &= (k_\mathrm{p} + k_\mathrm{m})C_\mathrm{m}\phi M - \frac{FD_1}{V}
\end{aligned} \tag{48}$$

The reaction rate constants $k_\star$ for termination by coupling (c), disproportionation (d), initiation (i), propagation (p) and chain

**Table 1**
Parameters and nominal input and state values for the polymerization reactor system.

| Par. | Value | Par. | Value |
|---|---|---|---|
| $A_c$ | $3.8223 \times 10^{10}$ kmol/(m$^3$ · h) | $f^*$ | 0.58 |
| $A_d$ | $3.1457 \times 10^{11}$ kmol/(m$^3$ · h) | $F$ | 1.00 m$^3$/h |
| $A_i$ | $3.7920 \times 10^{18}$ h$^{-1}$ | $\rho$ | 866 kg/m$^3$ |
| $A_p$ | $1.7700 \times 10^{9}$ kmol/(m$^3$ · h) | $C_{i,in}$ | 6.0 kmol/m$^3$ |
| $A_m$ | $1.0067 \times 10^{15}$ kmol/(m$^3$ · h) | $R$ | 8.314 J/(mol · K) |
| $E_c$ | 2944.2 kJ/kmol | $\Delta H_p$ | −57.8 kJ/mol |
| $E_d$ | 2944.2 kJ/kmol | $V$ | 0.1 m$^3$ |
| $E_i$ | 128770 kJ/kmol | $M$ | 100.12 kg/kmol |
| $E_p$ | 18283 kJ/kmol | $c_p$ | 2.0 kJ/(kg · K) |
| $E_m$ | 74478 kJ/kmol | $T_w$ | 293.2 K |
| $U$ | 720 kJ/(h · K · m$^2$) | $A$ | 2.0 m$^2$ |
| $c_w$ | 4.2 kJ/(kg · K) | $\rho_w$ | $10^3$ kg/m$^3$ |
| $V_w$ | 0.02 m$^3$ | | |
| Input | Nominal value | Input | Nominal value |
| $F_i$ | 0.01679 m$^3$/h | $F_w$ | 3.26363 m$^3$/h |
| State | Nominal value | State | Nominal value |
| $C_m$ | 7.7697 kg/kmol | $C_i$ | 0.1143 kg/kmol |
| $T$ | 329.98 K | $T_j$ | 296.67 K |
| $D_0$ | $3.5155 \times 10^{-4}$ kmol/m$^3$ | $D_1$ | 23.061 kg/m$^3$ |
| Disturbance | Nominal value | Disturbance | Nominal value |
| $C_{m,in}$ | 8.0 kmol/m$^3$ | $T_{in}$ | 350 K |

transfer to monomer (m) are expressed in the form of Arrhenius law:

$$k_\star = A_\star \exp(-E_\star/RT). \tag{49}$$

The molar fraction of live monomer chains $\phi$ is specified by the quasi-equilibrium assumption:

$$\phi = \sqrt{\frac{2f^* C_i k_i}{k_d + k_c}}. \tag{50}$$

The parameters and nominal states are given in Table 1. The inputs, outputs, disturbed variables and time are translated with the corresponding nominal values (so that the origin is the steady state to be regulated at) and scaled by 0.001 m$^3$/h, 1 m$^3$/h, 1000 kg/kmol, 1 K, 1 kmol/m$^3$, 1 K and 0.1 h, respectively.

### 4.2. Data generation and dissipativity learning

The trajectory samples are generated using random walks. Independent Wiener processes of random magnitudes uniformly distributed in [0,1] are assigned to $u_1$, $u_2$, $d_1$ and $d_2$ in the time interval [0,1] to simulate the system starting from the origin. 3000 independent trajectories are sampled, from which the dual dissipativity parameters $\Gamma^p$ are calculated by (27). With 2 disturbances, 2 control inputs and 2 outputs, each $\Gamma^p$ is a symmetric $r$-th order matrix ($\Gamma \in \mathbb{S}^r$) with $r = 6$. We choose the orthonormal bases ($r(r+1)/2 = 21$ in total) for $\mathbb{S}^r$ according to

$$E_{\frac{1}{2}(2r-i)(i-1)+j,kl} = \begin{cases} \delta_{kl}/\sqrt{r}, & i = j = 1 \\ \delta_{kl}/\sqrt{i(i-1)}, & i = j \neq 1, k < i \\ -(i-1)\delta_{kl}/\sqrt{i(i-1)}, & i = j \neq 1, k = i \\ 0, & i = j \neq 1, k > i \\ (\delta_{ik}\delta_{jl} + \delta_{il}\delta_{jk})/\sqrt{2}, & i \leq j \end{cases} \tag{51}$$

for $1 \leq i \leq j \leq r$ and $1 \leq k, l \leq r$ to vectorize the matrices $\Gamma^p$ into $\gamma^p \in \mathbb{R}^{21}$, where the Kronecker's $\delta$ symbol $\delta_{kl}$ for any two subscripts $k$ and $l$ equals 1 if $k = l$ and 0 otherwise.

We first pick the number of independent components $J$ equal to the dimension of sample vectors, i.e., $J = r(r+1)/2 = 21$ for ICA. Subplots 2–22 in Fig. 3 show the histograms of the obtained components for all the samples, with the probability density function of their inferred bi-exponential distributions shown as red curves, respectively. The accordingly computed samples of the lumped random variable $\zeta$ as defined in (36) and its inferred distribution are shown in the first subplot of Fig. 3. It is observed that compared to the inferred bi-exponential distribution, the empirical distribution of the samples has apparently higher densities near the centers ($c_j$ in (31)) but lower densities at moderate distances from the centers. To keep the empirical and the inferred distributions having the same variance equal to 1, the empirical distributions have longer tails than the inferred distributions. The deviations in $\eta_j$ result in the significant difference between the empirical and inferred distributions of $\zeta$. In principle, if our aim is only to capture the dissipative property of the system based on the data samples, we may seek to modify the bi-exponential distribution by asymmetric generalized normal distributions:

$$q_j(\eta_j) = \begin{cases} w_j \mu_j \exp(-a_j|\eta_j - c_j|^{\alpha_j}), & \eta_j \geq c_j \\ (1-w_j)\nu_j \exp(-b_j|\eta_j - c_j|^{\alpha_j}), & \eta_j < c_j \end{cases} \tag{52}$$

with smaller powers $\alpha_j < 1$ and optimized parameters $a_j$, $b_j$, $c_j$, $w_j$ and normalizing constants $\mu_j$, $\nu_j$. However, when $\alpha_j < 1$, the confidence region obtained by the lumped random variable $\eta = \sum_{j=1}^{J} a_j|\eta_j - c_j|^{\alpha_j}$ is not a convex set, and will cause computational intractability of the dissipativity learning control problem (45) or (47). Unfortunately, this does not seem to improve by changing the number of independent components $J$.

After ICA, we construct the polyhedral estimations of the dual dissipativity set and subsequently the dissipativity set as in (41). Since the empirical distribution of $\zeta$ is different from an Erlang or normal distribution, the confidence level $\Delta$ needs to be assigned according to the empirical distribution of $\zeta$ rather than using the properties of the Erlang or normal distributions such as the $3\sigma$ rule of thumb. Instead, due to the long-tail feature, we should make $\Delta$ larger than the corresponding value to the desired confident level under the Erlang or normal distribution. For example, if we need to cover 95% of the samples, the empirical distribution requires to choose $\Delta \geq 6.5762$, which is significantly higher than the value of 1.6449 required by the normal distribution $\mathcal{N}(1, J^{-1/2})$.

For $J = 21$ and $\Delta$ corresponding to 95% of the samples, we found that the origin is an interior point of $\mathcal{S}_\Delta$ and therefore $\mathcal{S}_\Delta^*$ is a singleton of $\Pi = 0$, which is physically meaningless since the supply rate and hence the storage function are constantly zero. This can be avoided only when $\Delta$ is as small as to cover 2% of the samples, which fails to capture the true input–output response of the system. Therefore, the independent component number $J$ must be well-tuned so that a meaningful dissipativity set can be generated under a sufficiently high confidence level $\Delta$. For this, we vary $J$ and always set $\Delta$ at the value to cover 95% of the $\zeta$ samples. For each $J$, we find the element $\Pi \in \mathcal{S}_\Delta^*$ that minimizes the leading eigenvalue of the output blocks:

$$\begin{aligned} \min_{\Pi} \quad & \rho_{\max}(\Pi_{\tilde{y},\tilde{y}}) \\ \text{s.t.} \quad & \Pi \in \mathcal{S}_\Delta^*, \quad \operatorname{trace}(\Pi_{d\tilde{u},d\tilde{u}}) = 1 \end{aligned} \tag{53}$$

where the last constraint is imposed for a fair comparison since $\mathcal{S}_\Delta^*$ is a cone. The $\Pi$ thus determined can be roughly considered as the least conservative estimate of the dissipativity matrix. Their traces are compared in Table 2.

From Table 2 we observe that both too large and too small numbers of independent components are undesirable. On one hand, when $J$ is large, the dissipativity learning procedure to construct the dual dissipativity set $\mathcal{S}_\Delta$ takes into consideration insignificant dimensions of the data samples, and results in an overly conservative estimation of $\mathcal{S}_\Delta$ (i.e. the constructed polyhedron is much larger than it need be), thus making its dual cone $\mathcal{S}_\Delta^*$ too small (which reduces to a singleton when $J = 20$ or 21). On the other hand, if $J$ is too small, important dimensions of the data are

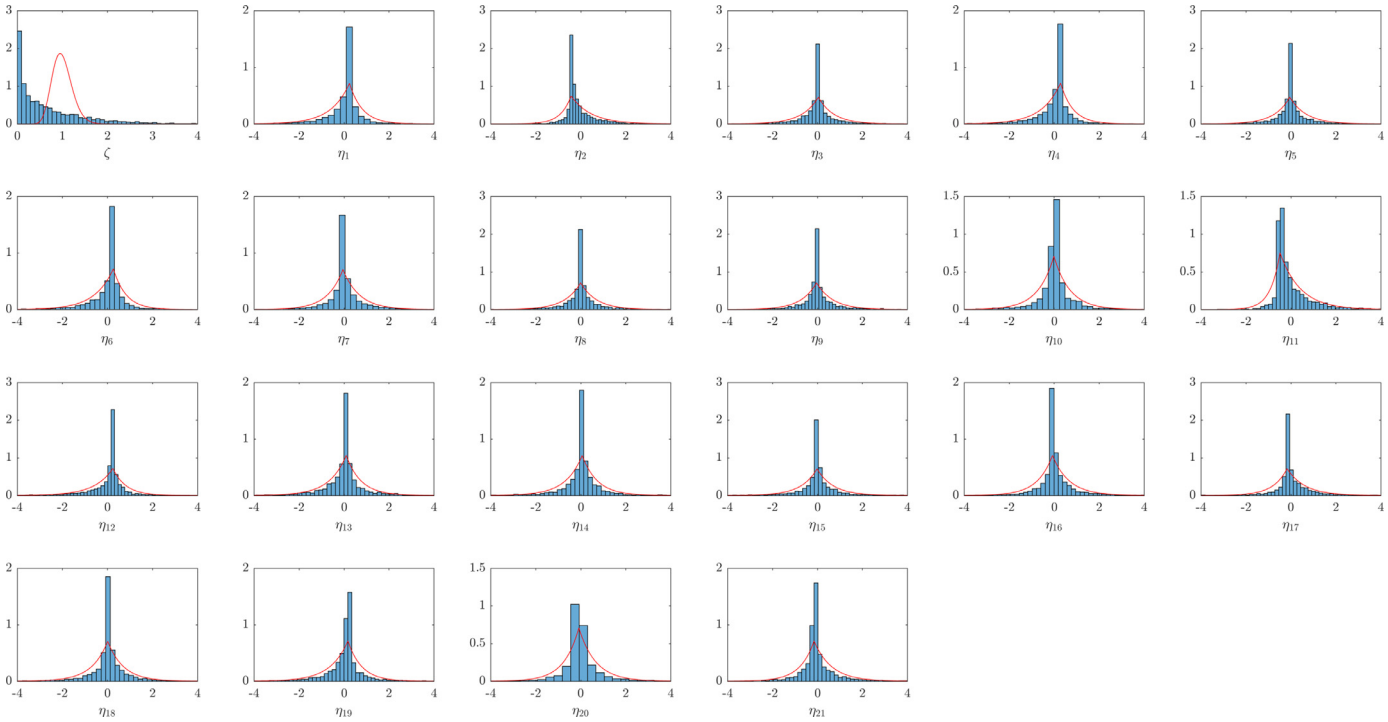


**Fig. 3.** Distribution of the independent component parameters and the lumped random variable $\zeta$ when $J = 21$ for the polymerization reactor.

**Table 2**
Minimized leading eigenvalue of the output blocks of the dissipativity matrix $\Pi$ under different numbers of independent components.

| | | | | |
|---|---|---|---|---|
| $J$ | 7 | 8 | 9 | 10 |
| $\rho_{\max}(\Pi_{\tilde{y},\tilde{y}})$ | $-\infty$ | $-\infty$ | −0.5917 | −0.4034 |
| $J$ | 11 | 12 | 13 | 14 |
| $\rho_{\max}(\Pi_{\tilde{y},\tilde{y}})$ | −0.4022 | −0.3923 | −0.3227 | −0.1476 |
| $J$ | 15 | 16 | 17 | 18 |
| $\rho_{\max}(\Pi_{\tilde{y},\tilde{y}})$ | −0.0689 | −0.0684 | 0.3099 | 0.3964 |
| $J$ | 19 | 20 | 21 | |
| $\rho_{\max}(\Pi_{\tilde{y},\tilde{y}})$ | 0.5324 | $+\infty$ | $+\infty$ | |

ignored, and hence the dissipativity learning does not responsibly capture the system dynamics and gives naively radical estimates, such as in the case of $J = 7$ or 8, when $\mathcal{S}_{\Delta}^{*}$ allows a dissipativity matrix with $\Pi_{d\tilde{u},d\tilde{u}} = 0$ and $\Pi_{\tilde{y},\tilde{y}} \prec 0$, meaning that the storage can not increase anyhow. When $J = 10$, 11 and 12, the minimized $\rho_{\max}(\Pi_{\tilde{y},\tilde{y}})$ results are similar, which suggest a proper range of $J$. This can be further justified by the covariance matrix of the samples $\gamma^p$, $p = 1, \ldots, P$:

$$\Sigma = \frac{1}{P-1}\sum_{p=1}^{P}(\gamma^p - \bar{\gamma})(\gamma^p - \bar{\gamma})^{\top}, \tag{54}$$

whose 11th eigenvalue in descending order, 0.0059, is an order-of-magnitude smaller than the 10th eigenvalue 0.0572, and the eigenvalues after the 13th are smaller than 1% of the leading eigenvalue, 0.1944, implying that there are about 10–13 orthogonal dimensions in which the data variations significantly exist.

### 4.3. Controller design and simulation

Now we use different values of $J$ between 10 and 13 and different values of $\Delta$ to cover different percentages of the data samples, and solve the $L_2$-optimal P control problem (45) to obtain the guaranteed upper bounds of the squared $L_2$-gain, $\beta$. The results are shown in Table 3. It can be observed that $J$ should be chosen as 11 or 12, so that the confidence level $\Delta$ can be found to have a non-trivial effect on the control performance. Since $J = 11$ gives lower upper bound on the $L_2$-gain than the other 3 values of $J$, in the sequel we set $J = 11$.

**Table 3**
Optimal control performances ($\beta$) under different number of independent components and confidence levels for the polymerization reactor.

| $\Delta$ | 85% | 90% | 95% | 98% | 99% |
|---|---|---|---|---|---|
| $J = 10$ | 0.1919 | 1.5152 | 1.5152 | 1.5152 | 1.5152 |
| $J = 11$ | 0.4755 | 0.4844 | 0.5275 | 0.5586 | 0.5783 |
| $J = 12$ | 0.7323 | 0.7589 | 0.7904 | 0.8139 | 0.8297 |
| $J = 13$ | 5.3541 | 5.3541 | 5.3541 | 5.3541 | 5.3541 |

When the degree of polymerization (reflecting the rate of reactions) and the temperature deviate from their setpoints, since the reaction rates increase with temperature and the reactions are exothermic, the deviations with opposite (same) signs annihilate (exacerbate) each other to approach (escape) the setpoints, resulting in a decrease (an increase) of the storage function. To reflect this dynamic feature of the system, the output block $\Pi_{\tilde{y},\tilde{y}}$ should have one negative eigenvalue whose associated eigenvector has two components with opposite signs, and one positive eigenvalue whose associated eigenvector lies in the first quadrature. Also, the controller gain $K$ should have 4 positive elements so that the controller signals are small when the output deviations have the same signs and large when the output deviations are opposite. We note that this is true for the optimized results obtained from the $L_2$-optimal controller problem (45), e.g., when the confidence level is 95%, we have

$$K = \begin{bmatrix} 1.5424 & 2.1511 \\ 1.0371 & 0.7978 \end{bmatrix} \tag{55}$$

and

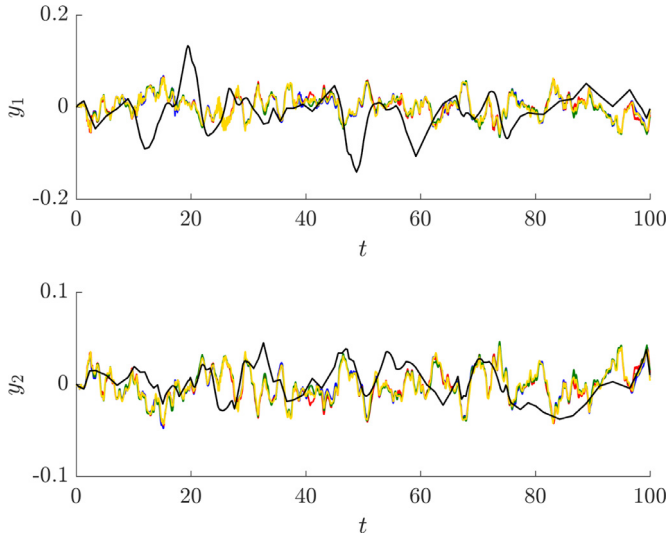


**Fig. 4.** Process simulation for dissipativity learning controllers under disturbances. The blue, red, green, and yellow lines correspond to confidence levels 85%, 90%, 95% and 99%, respectively, under $J = 11$. The black lines correspond to the open-loop system ($u = 0$). (For interpretation of the references to colour in this figure legend, the reader is referred to the web version of this article.)

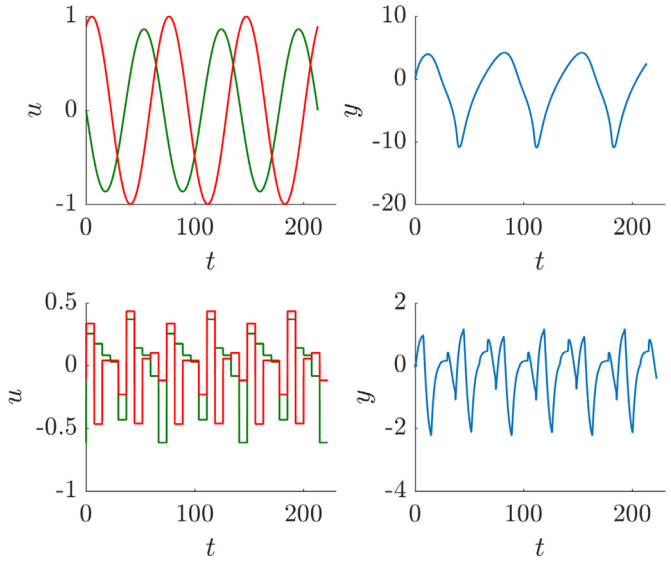


**Fig. 5.** Desired input and output trajectories the oscillatory reactor operated periodically under sinusoidal (upper subplots) and piecewise constant inputs (lower subplots). Red and green curves correspond to $u_1$ and $u_2$, respectively. (For interpretation of the references to colour in this figure legend, the reader is referred to the web version of this article.)

$$\Pi = \begin{bmatrix} 0.3970 & 0.1460 & 0.4864 & -0.2130 & -0.3465 & -1.6909 \\ 0.1460 & 0.3642 & 0.6708 & -1.0100 & -0.1917 & 0.2739 \\ 0.4864 & 0.6708 & 1.3754 & -1.7372 & -1.8620 & -3.7239 \\ -0.2130 & -1.0100 & -1.7372 & 2.9100 & -1.3759 & 0.6174 \\ -0.3465 & -0.1917 & -1.8620 & -1.3759 & 3.0431 & 6.2436 \\ -1.6909 & 0.2739 & -3.7239 & 0.6174 & 6.2436 & 1.4358 \end{bmatrix}. \tag{56}$$

The same physical explanations can be made for $\Pi_{\tilde{u},\tilde{u}}$ and $\Pi_{d,d}$. The eigenvectors associated with the larger eigenvalue of $\Pi_{\tilde{u},\tilde{u}}$ and $\Pi_{d,d}$ should have opposite signs and same signs, respectively, since the two control inputs have opposite effects (feeding initiator accelerates polymerization while cooling water decelerates reactions) and the two disturbances have the same effects (increasing monomer feed and increasing feed temperature both accelerate reactions). These physical requirements are satisfied by the obtained $\Pi$ with $\Pi_{\tilde{u}_1,\tilde{u}_2} < 0$ and $\Pi_{d_1,d_2} > 0$.

We simulate the dissipativity learning controllers obtained under confidence levels 85%, 90%, 95% and 99%, along with the open-loop system with feedback gain equal to the zero matrix. The disturbance signals $d_1$ and $d_2$ that we use are two independent zero-mean Orstein-Uhlenbeck processes, defined as

$$dU = -\omega U dt + \upsilon dW, \quad U(0) = 0, \tag{57}$$

where $dW$ denotes the Wiener process, and $\upsilon = 0.1$, $\omega = 6$ (corresponding to a time constant of 1/6 time scales or 1 min). Fig. 4 shows the simulated output trajectories within 100 time scales (10 hours). Apparently, compared to the open-loop system, the learned controllers have a better performance of disturbance rejection, with the outputs (degree of polymerization and reactor temperature) kept close to the setpoints and free from long-lasting significant deviations.

Of course, the use of a P controller in this case study is only for the illustration of how the dissipativity learning control method can give well-performing controllers with reasonable physical interpretations of the controller gains. P controllers may be not suitable and an offset will be expected if the setpoint of the process can vary with time. In such cases, one may consider designing a dissipativity-based PID controller, as illustrated in the next case study.

## 5. Case study: Dissipativity learning tracking control of an oscillatory reactor

In this section we apply the proposed dissipativity learning control method to the tracking control of a CSTR (Özgülşen et al., 1992) in which the catalyzed gas phase oxidization of ethylene takes place. There exist two side reactions to oxidize the primary product – ethylene oxide – and the reactant ethylene into carbon dioxide. It is known that appropriate periodic operation of this reactor can be economically more favorable than the optimal steady-state operation (Chen et al., 1994).

### 5.1. System description

The state-space model involves 4 states and 2 inputs:

$$\begin{aligned}
\dot{x}_1 &= (0.35 + u_1)(1 - x_1 x_4) \\
\dot{x}_2 &= (0.35 + u_1)(0.1 + u_2 - x_2 x_4) - A_1 \exp(C_1/x_4)(x_2 x_4)^{0.5} \\
&\quad - A_2 \exp(C_2/x_4)(x_2 x_4)^{0.25} \\
\dot{x}_3 &= -(0.35 + u_1)x_3 x_4 + A_1 \exp(C_1/x_4)(x_2 x_4)^{0.5} \\
&\quad - A_3 \exp(C_3/x_4)(x_3 x_4)^{0.5} \\
\dot{x}_4 &= x_1^{-1}[(0.35 + u_1)(1 - x_4) + B_1 \exp(C_1/x_4)(x_2 x_4)^{0.5} \\
&\quad + B_2 \exp(C_2/x_4)(x_2 x_4)^{0.25} + B_3 \exp(C_3/x_4)(x_3 x_4)^{0.5} \\
&\quad - B_4(x_4 - 1 - d)]
\end{aligned} \tag{58}$$

The 4 states ($x_1$, $x_2$, $x_3$, $x_4$) are the dimensionless density, ethylene concentration, ethylene oxide concentration, and temperature, respectively. The gas phase flow rate and the ethylene concentration at the reactor inlet are used as control inputs. We assume that there is a disturbance $d$ in the cooling water temperature. The nominal steady states under zero inputs and disturbances are

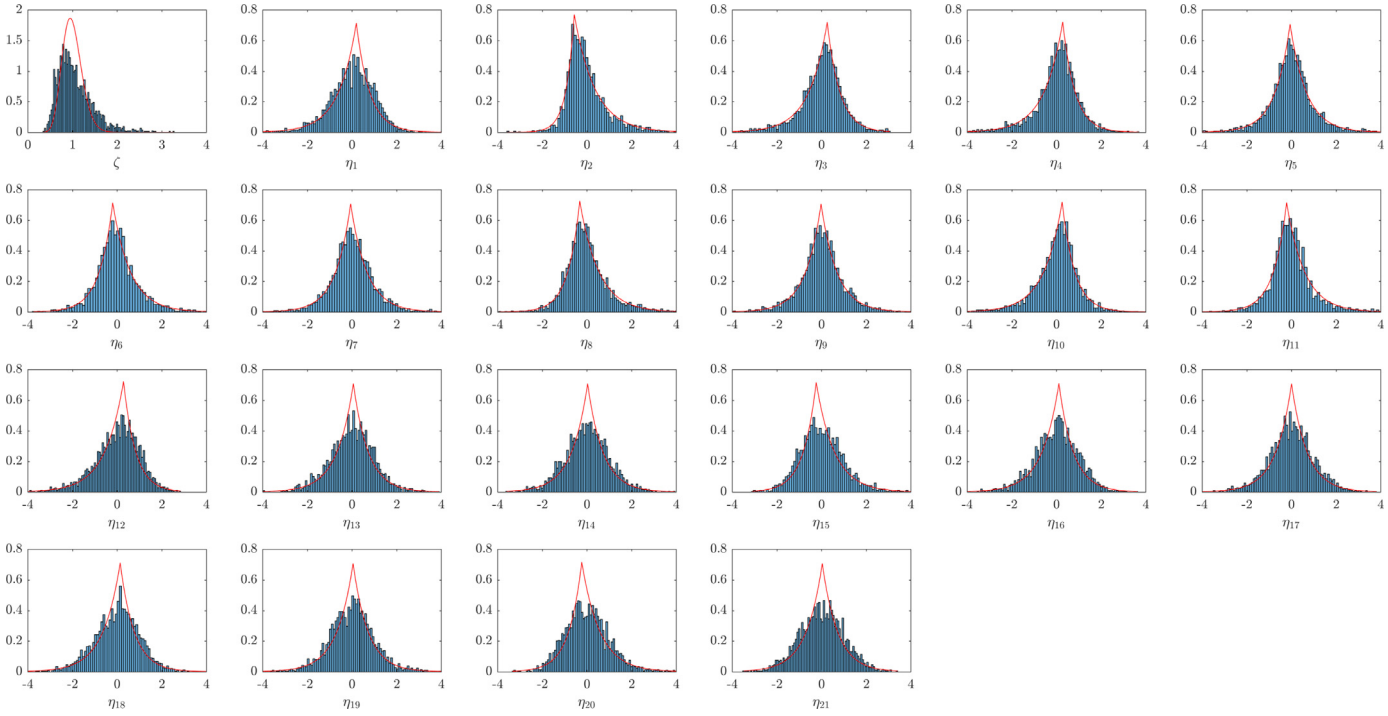


**Fig. 6.** Trajectory samples of the oscillatory reactor system.

**Table 4**
Parameters and nominal steady state for the oscillatory reactor system.

| Par. | Value | Par. | Value |
|---|---|---|---|
| $A_1$ | 92.80 | $B_1$ | 7.32 |
| $A_2$ | 12.66 | $B_2$ | 10.39 |
| $A_3$ | 2412.71 | $B_3$ | 2170.5 |
| $C_1$ | −8.13 | $B_4$ | 7.02 |
| $C_2$ | −7.12 | $C_3$ | −11.07 |
| State | Value | State | Value |
| $x_1^{ss}$ | 0.99889 | $x_2^{ss}$ | 0.06494 |
| $x_3^{ss}$ | 0.00949 | $x_4^{ss}$ | 1.00111 |

given in Table 4. The reactor temperature is taken as the output ($y = x_4 - x_4^{ss}$). The inputs $u_1$ and $u_2$, disturbance $d$, and output $y$ are then scaled by 0.35, 0.10, 0.0001 and 0.0001, respectively.

Chen et al. (1994) identified for $d = 0$ the optimal operation under control inputs in sinusoidal and piecewise constant forms, whose concrete forms are omitted here for brevity and the resulting trajectories are illustrated in Fig. 5. In this section we assume that these two sets of trajectories are available without model knowledge, and examine whether the proposed dissipativity learning control method can efficiently track them. For tracking control where the desired inputs and the output oscillate over considerable ranges, it may not be sufficient to use P controllers. Hence we consider dissipativity learning with expanded outputs with integral and derivative of $y$, and controller design in the formulation of (47).

### 5.2. Data generation and dissipativity learning

Independent trajectories ($P = 2500$) are sampled in a similar way as in Section 4. For each sample, zero-mean stochastic processes bounded in $[-1, 1]$ with a modified Orstein-Uhlenbeck form:

$$dU = -\frac{\omega U}{1 - U^4} dU + \sigma\, dW \tag{59}$$

($\omega = 1,\ \sigma = 1$) are used to generate $\bar{u}(t)$ and $u(t)$, and a standard Wiener process is used to generate $d(t)$ within a time scale to drive the plant from the nominal steady state, yielding the trajectory of $(\tilde{y}_P, \tilde{y}_I, \tilde{y}_D)$, $(y_P, y_I, y_D)$ and $(\tilde{y}_P, \tilde{y}_I, \tilde{y}_D)$ by subtraction. Since the output derivatives are used in dissipativity learning, the output signals need to be smooth enough. For this purpose, Savitzky-Golay filters (Savitzky and Golay, 1964) of order 3 with a frame length of 0.5 time scale are applied to the disturbance and inputs. 100 of these trajectories are shown in Fig. 6. From the trajectories, the dual dissipativity parameters $\Gamma^p$ are calculated.

The distributions of independent components $\eta_j,\ j = 1, \ldots, J$ under $J = 21$ are shown in Fig. 7. It can be expected that compared with the polymerization reactor example, the $\Gamma^p$ data samples from the oscillatory reactor can be better described by the bi-exponential distributions of its independent components. This is due to the higher extent of dispersion of independent components from their distribution centers, which may be explained by the fact that the data are sampled from a wide range of trajectories to track rather than a single steady state to regulate at. The approach to determine the appropriate range of $J$ is similar to the previous case study, i.e., we perform the dissipativity learning step under a series of different values of $J$ and check whether solving (53) returns a negative feasible solution. We then calculate the covariance matrix (54) to choose the number of eigenvalues greater than 1% of the leading eigenvalue, which suggests that $J = 5$.

### 5.3. Controller design and simulation

Finally we solve the $L_2$-optimal dissipativity learning PID control problem (47) under $J = 5$ and confidence levels $\Delta$ corresponding to 85%, 90%, 95% and 99% of the samples. For example, under the confidence level of 95% of the samples, the learned PID controller is

$$\begin{aligned} \tilde{u}_1 &= 2.4407\tilde{y}_P + 0.2008\tilde{y}_I + 0.1410\tilde{y}_D, \\ \tilde{u}_2 &= -4.7141\tilde{y}_P - 1.2145\tilde{y}_I - 0.2655\tilde{y}_D. \end{aligned} \tag{60}$$

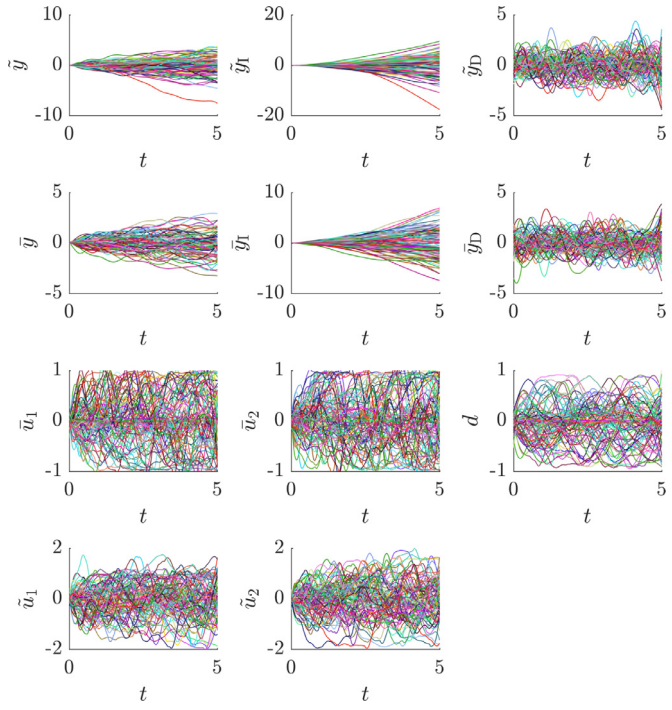

**Fig. 7.** Distribution of the independent components and the lumped random variable $\zeta$ when $J = 21$ for the oscillatory reactor.

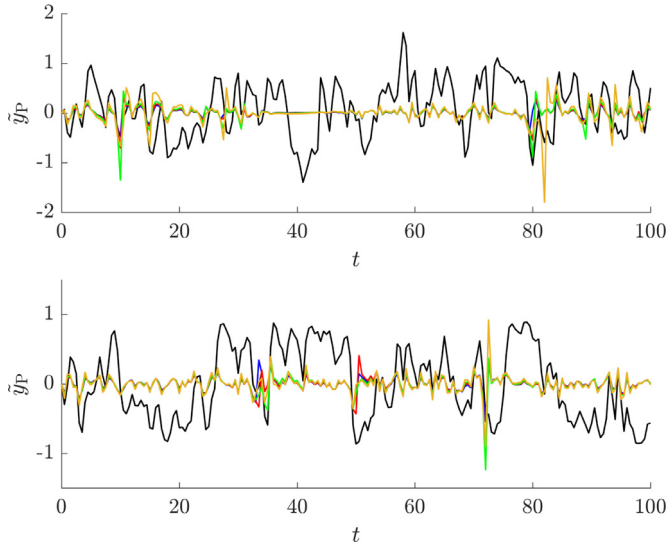

**Fig. 8.** Simulated signals of the output errors of tracking the periodic trajectories. The upper and lower subplots correspond to the trajectories in Fig. 5 with sinusoidal and piecewise constant signals, respectively. The blue, red, green, and yellow lines correspond to dissipativity learning controllers obtained under $J = 5$ and confidence levels 85%, 90%, 95% and 99%, respectively. The black lines correspond to the open-loop system ($u = 0$). (For interpretation of the references to colour in this figure legend, the reader is referred to the web version of this article.)

The negative gains for the second input reflect the cooling effect on the reactor temperature of the cooling water. The positive gains for the second input result from the fact that increasing (decreasing) the gas phase flow rate decreases (increases) the residence time, thus decreasing (increasing) the reactor temperature with a lower (higher) extent of exothermic reactions.

A stochastic Orstein-Uhlenbeck process is generated as the disturbance signal. The simulated trajectories under the obtained 4 controllers and the open-loop trajectories are shown in Fig. 8. It becomes apparent that under the learned controllers, the disturbance is well attenuated compared to the open-loop system, where the disturbance results in large fluctuations of the output.

## 6. Conclusions

Dissipativity, as an important characterization of the input–output response of dynamic systems, can be leveraged in the setting of input–output data-driven control. Specifically, with the trajectories sampled from the dynamics, we can learn the range of the parameters in the supply rate function (dissipativity set), based on which a dissipative controller can be synthesized to shape the closed-loop stability. In this work, we first pointed that such a dissipativity learning method is applicable to both regulating and tracking control, and then proposed a method of learning dissipativity and synthesizing dissipativity-based controllers from trajectory data based on independent component analysis and distribution estimation. Two chemical reactor systems are used for detailed case studies that demonstrated the efficacy of our proposed method. The P and PID controllers designed with the proposed method achieve satisfactory performance. In addition, we have shown that the learned dissipativity parameters are of good physical interpretability, based on which the signs of the optimal controller gains are found to be in accordance with the physical relations among the process variables.

Although tested with only a few case studies so far, this framework is promising for wider application of input–output data-driven control on process systems, including those governed by partial differential and differential-algebraic equations, and large-scale processes. We note that as a machine learning-based approach, the performance of dissipativity learning control is essentially dependent on the accuracy of the dissipativity learning result. To better guarantee the learning performance, there are two open problems yet to be explored in future research, namely how to optimally generate or select data samples, and how to perform learning when data are less satisfactory, e.g., when sufficient open-loop trajectories are not available.

## Declaration of Competing Interest

The authors whose names are listed immediately below certify that they have NO affiliations with or involvement in any organization or entity with any financial interest (such as honoraria; educational grants; participation in speakers' bureaus; membership, employment, consultancies, stock ownership, or other equity interest; and expert testimony or patent-licensing arrangements), or non-financial interest (such as personal or professional relationships, affiliations, knowledge or beliefs) in the subject matter or materials discussed in this manuscript.

## Acknowledgment

This work was supported by National Science Foundation (NSF-CBET) and a Doctoral Dissertation Fellowship (DDF) of University of Minnesota for Wentao Tang.

## References

Aggelogiannaki, E., Sarimveis, H., 2008. Nonlinear model predictive control for distributed parameter systems using data driven artificial neural network models. Comput. Chem. Eng. 32 (6), 1225–1237.
Alonso, A.A., Ydstie, B.E., 1996. Process systems, passivity and the second law of thermodynamics. Comput. Chem. Eng. 20, S1119–S1124.
Bao, J., Lee, P.J., 2007. Process Control: The Passive Systems Approach. Springer.
Chen, C.-C., Hwang, C., Yang, R.Y.K., 1994. Optimal periodic forcing of nonlinear chemical processes for performance improvements. Can. J. Chem. Eng. 72 (4), 672–682.

Chi, R., Hou, Z., Huang, B., Jin, S., 2015. A unified data-driven design framework of optimality-based generalized iterative learning control. Comput. Chem. Eng. 77, 10–23.
Daoutidis, P., Soroush, M., Kravaris, C., 1990. Feedforward/feedback control of multivariable nonlinear processes. AIChE J. 36 (10), 1471–1484.
García-Sandoval, J.P., Hudon, N., Dochain, D., Gonzalez-Alvarez, V., 2016. Stability analysis and passivity properties of a class of thermodynamic processes: an internal entropy production approach. Chem. Eng. Sci. 139, 261–272.
Ghavamzadeh, M., Mannor, S., Pineau, J., Tamar, A., 2015. Bayesian reinforcement learning: a survey. Found. Trends Mach. Learn. 8 (5–6), 359–483.
Grant, M., Boyd, S., 2014. CVX: Matlab software for disciplined convex programming, version 2.1. http://cvxr.com/cvx.
Hangos, K.M., Bokor, J., Szederkényi, G., 2001. Hamiltonian view on process systems. AIChE J. 47 (8), 1819–1831.
Heirung, T.A.N., Ydstie, B.E., Foss, B., 2017. Dual adaptive model predictive control. Automatica 80, 340–348.
Hill, D., Moylan, P., 1976. The stability of nonlinear dissipative systems. IEEE Trans. Autom. Control 21 (5), 708–711.
Hill, D.J., Moylan, P.J., 1980. Dissipative dynamical systems: basic input-output and state properties. J. Franklin Inst. 309 (5), 327–357.
Hioe, D., Bao, J., Ydstie, B.E., 2013. Dissipativity analysis for networks of process systems. Comput. Chem. Eng. 50, 207–219.
Hou, Z.-S., Wang, Z., 2013. From model-based control to data-driven control: survey, classification and perspective. Inf. Sci. 235, 3–35.
Hyvärinen, A., Oja, E., 2000. Independent component analysis: algorithms and applications. Neural Netw. 13 (4–5), 411–430.
Khalil, H.K., 2002. Nonlinear systems, 3rd Pearson.
Korda, M., Mezić, I., 2018. Linear predictors for nonlinear dynamical systems: koopman operator meets model predictive control. Automatica 93, 149–160.
Lao, L., Ellis, M., Christofides, P.D., 2013. Economic model predictive control of transport-reaction processes. Ind. Eng. Chem. Res. 53 (18), 7382–7396.
Lee, J.H., Wong, W., 2010. Approximate dynamic programming approach for process control. J. Process Control 20 (9), 1038–1048.
Lee, J.M., Lee, J.H., 2005. Approximate dynamic programming-based approaches for input–output data-driven control of nonlinear processes. Automatica 41 (7), 1281–1288.
Lillicrap, T.P., Hunt, J.J., Pritzel, A., Heess, N., Erez, T., Tassa, Y., Silver, D., Wierstra, D., 2015. Continuous control with deep reinforcement learning. arXiv preprint. ArXiv:1509.02971
Lozano, R., Brogliato, B., Egeland, O., Maschke, B., 2013. Dissipative Systems Analysis and Control: Theory and Applications. Springer.
Luo, B., Wu, H.-N., Huang, T., Liu, D., 2014. Data-based approximate policy iteration for affine nonlinear continuous-time optimal control design. Automatica 50 (12), 3281–3290.
Maupong, T., Mayo-Maldonado, J.C., Rapisarda, P., 2017. On Lyapunov functions and data-driven dissipativity. IFAC-PapersOnLine 50 (1), 7783–7788. 20th IFAC World Congress
Mesbah, A., 2018. Stochastic model predictive control with active uncertainty learning: a survey on dual control. Annu. Rev. Control 45, 107–117.
Moylan, P., Hill, D., 1978. Stability criteria for large-scale systems. IEEE Trans. Autom. Control 23 (2), 143–149.
Mu, C., Ni, Z., Sun, C., He, H., 2017. Data-driven tracking control with adaptive dynamic programming for a class of continuous-time nonlinear systems. IEEE Trans. Cybern. 47 (6), 1460–1470.
Narasingam, A., Kwon, J.S.-I., 2018. Data-driven identification of interpretable reduced-order models using sparse regression. Comput. Chem. Eng. 119, 101–111.
Narasingam, A., Kwon, J.S.-I., 2019. Koopman Lyapunov-based model predictive control of nonlinear chemical process systems. AIChE J. 0, e16743. In press
Ning, C., You, F., 2018. Data-driven decision making under uncertainty integrating robust optimization with principal component analysis and kernel smoothing methods. Comput. Chem. Eng. 112, 190–210.
Özgülşen, F., Adomaitis, R.A., Çinar, A., 1992. A numerical method for determining optimal parameter values in forced periodic operation. Chem. Eng. Sci. 47 (3), 605–613.
Parzen, E., 1962. On estimation of a probability density function and mode. Ann. Math. Stat. 33 (3), 1065–1076.
Polushin, I.G., Fradkov, A.L., Hill, D.J., 2000. Passivity and passification of nonlinear systems. Autom. Remote Control 61 (3), 355–388.
Proctor, J.L., Brunton, S.L., Kutz, J.N., 2018. Generalizing Koopman theory to allow for inputs and control. SIAM J. Appl. Dyn. Syst. 17 (1), 909–930.
Qin, S.J., Chiang, L.H., 2019. Advances and opportunities in machine learning for process data analytics. Comput. Chem. Eng. 126, 465–473.
Ramirez, H., Maschke, B., Sbarbaro, D., 2013. Irreversible port-Hamiltonian systems: a general formulation of irreversible processes with application to the CSTR. Chem. Eng. Sci. 89, 223–234.
Romer, A., Montenbruck, J.M., Allgöwer, F., 2017. Determining dissipation inequalities from input-output samples. IFAC-PapersOnLine 50 (1), 7789–7794. 20th IFAC World Congress
Ruff, L., Görnitz, N., Deecke, L., Siddiqui, S.A., Vandermeulen, R., Binder, A., Müller, E., Kloft, M., 2018. Deep one-class classification. Proc. Mach. Learn. Res. 80, 4393–4402. Proc. 35th Intl. Conf. Mach. Learn. (ICML)
Ruszkowski, M., Garcia-Osorio, V., Ydstie, B.E., 2005. Passivity based control of transport reaction systems. AIChE J. 51 (12), 3147–3166.
Savitzky, A., Golay, M.J.E., 1964. Smoothing and differentiation of data by simplified least squares procedures. Anal. Chem. 36 (8), 1627–1639.
Schölkopf, B., Smola, A.J., 2002. Learning with Kernels: Support Vector Machines, Regularization, Optimization, and Beyond. MIT Press.
Shen, X., Diamond, S., Udell, M., Gu, Y., Boyd, S., 2017. Disciplined multi-convex programming. In: 29th Chin. Control Decis. Conf. (CCDC). IEEE, pp. 895–900.
Shin, J., Badgwell, T.A., Liu, K.-H., Lee, J.H., 2019. Reinforcement learning – overview of recent progress and implications for process control. Comput. Chem. Eng. 127, 282–294.
Soroush, M., Kravaris, C., 1992. Nonlinear control of a batch polymerization reactor: an experimental study. AIChE J. 38 (9), 1429–1448.
Spielberg, S., Tulsyan, A., Lawrence, N.P., Loewen, P.D., Gopaluni, R.B., 2019. Towards self-driving processes: a deep reinforcement learning approach to control. AIChE J. 65 (10), e16689.
Tanaskovic, M., Fagiano, L., Novara, C., Morari, M., 2017. Data-driven control of nonlinear systems: an on-line direct approach. Automatica 75, 1–10.
Tang, W., Daoutidis, P., 2018. Distributed adaptive dynamic programming for data–driven optimal control. Syst. Control Lett. 120, 36–43.
Tang, W., Daoutidis, P., 2019. Input-output data-driven control through dissipativity learning. In: 2019 Annu. Am. Control Conf. (ACC), pp. 4217–4222.
Venkatasubramanian, V., 2019. The promise of artificial intelligence in chemical engineering: is it here, finally? AIChE J. 65 (2), 466–478.
Wahlberg, B., Syberg, M.B., Hjalmarsson, H., 2010. Non-parametric methods for $l_2$-gain estimation using iterative experiments. Automatica 46 (8), 1376–1381.
Willems, J.C., 1972. Dissipative dynamical systems. II. linear systems with quadratic supply rates. Arch. Ration. Mech. Anal. 45 (5), 352–393.
Williams, M.O., Kevrekidis, I.G., Rowley, C.W., 2015. A data–driven approximation of the Koopman operator: extending dynamic mode decomposition. J. Nonlin. Sci. 25 (6), 1307–1346.
Ydstie, B.E., 2002. Passivity based control via the second law. Comput. Chem. Eng. 26 (7–8), 1037–1048.
Zhang, Q., Grossmann, I.E., Sundaramoorthy, A., Pinto, J.M., 2016. Data-driven construction of convex region surrogate models. Optim. Eng. 17 (2), 289–332.